Design, Analysis, and Application of Architected Ferroelectric Lattice Materials

Amanda X. Wei

Thesis submitted to the faculty of the Virginia Polytechnic Institute and State University
in partial fulfillment of the requirements for the degree of

Master of Science
In
Mechanical Engineering

Xiaoyu (Rayne) Zheng, Chair
Jiangtao Cheng
Robert L. West

May 3, 2019
Blacksburg, Virginia

Keywords: architected lattice, ferroelectric materials, rational design

Design, Analysis, and Application of Architected Ferroelectric Lattice Materials

Amanda X. Wei

ABSTRACT

Ferroelectric materials have been an area of keen interest for researchers due to their useful electro-mechanical coupling properties for a range of modern applications, such as sensing, precision actuation, or energy harvesting. The distribution of the piezoelectric coefficients, which corresponds to the piezoelectric properties, in traditional crystalline ferroelectric materials are determined by their inherent crystalline structure. This restriction limits the tunability of their piezoelectric properties. In the present work, ferroelectric lattice materials capable of a wide range of rationally designed piezoelectric coefficients are achieved through lattice micro-architecture design. The piezoelectric coefficients of several lattice designs are analyzed and predicted using an analytical volume-averaging approach. Finite element models were used to verify the analytical predictions and strong agreement between the two sets of results were found. Select lattice designs were additively manufactured using projection microstereolithography from a PZT-polymer composite and their piezoelectric coefficients experimentally verified and also found to be in agreement with the analytical and numerical predictions. The results show that the use of lattice micro-architecture successfully decouples the dependency of the piezoelectric properties on the material's crystalline structure, giving the user a means to tune the piezoelectric properties of the lattice materials. Real-world application of a ferroelectric lattice structure is demonstrated through application as a multi-directional stress sensor.

Design, Analysis, and Application of Architected Ferroelectric Lattice Materials

Amanda X. Wei

GENERAL AUDIENCE ABSTRACT

Ferroelectric materials have been an area of keen interest for researchers due to their useful electro-mechanical coupling properties for a range of modern applications, such as sensing, precision actuation, or energy harvesting. However, the piezoelectric properties of traditional materials are not easily augmented due to their dependency on material crystalline structure. In the present work, material architecture is investigated as a means for designing new piezoelectric materials with tunable sets of piezoelectric properties. Analytical predictions of the properties are first obtained and then verified using finite element models and experimental data from additively manufactured samples. The results indicate that the piezoelectric properties of a material can in fact be tuned by varying material architecture. Following this, real-world application of a ferroelectric lattice structure is demonstrated through application as a multi-directional stress sensor.

ACKNOWLEDGEMENTS

I would like to thank my family and friends for their endless support and love. I would also like to thank my advisor, Dr. Xiaoyu (Rayne) Zheng for his insights, guidance, and support for my career goals. I thank my colleagues Huachen Cui, Desheng Yao, Ryan Hensleigh, and my other lab mates for their contributions to this work and also for their friendship. I would also thank my committee members, Dr. Jiangtao Cheng and Dr. Robert West for their help. Finally, I thank all the student, faculty, and professional mentors I have been fortunate to have up to this point.

Table of Contents

List of Figures

List of Tables

Chapter 1: Introduction

In the present work, a novel framework for the design and analysis of the piezoelectric coefficients of ferroelectric lattice materials is developed. Following this, real-world applications of a ferroelectric lattice material as a stress sensor is demonstrated. The motivation, hypothesis, and objective of this work are presented in the following introductory sections.

1.1. Motivation

The coupling between mechanical and electrical response exhibited by ferroelectric materials is highly useful in the modern electronics driven world. Ferroelectric materials are used in a range of devices including sensors[1], precision actuators[2], active vibration dampers[3], medical imaging devices[4], and energy harvesters[5]. The piezoelectric performance of these ferroelectric materials is characterized by their piezoelectric coefficients. Due to the variety of applications in which ferroelectrics are used, it may be desirable to tailor these coefficients for a specific purpose. For crystalline ferroelectric ceramics, some existing and popular methods of tuning these coefficients are through domain-engineering[6], chemical doping[7], or thermal tuning[8]. While their respective techniques vary, the overarching working principle behind each of these methods is modification of the crystalline structure or composition of the material[6][7][8]. As can be expected, minute changes to a material at such a fundamental level can result in drastic changes in not only piezoelectric property but other material properties as well, which may not always be desirable.

Ferroelectric ceramics can be used to create ferroelectric composite materials. Just as for pure crystalline ferroelectric ceramics, the piezoelectric properties of ferroelectric composites can be tuned. These tuning approaches are diverse due to the large variation in the composites themselves with respect to components, geometry, connectivity, and working principle[9]. This diversity is useful since the piezoelectric coefficients of each individual composite can typically only be augmented within a certain range. But the diversity among these composites means that the sum of the material property space covered by all the composites is large. However, the diversity in composite design also makes it difficult to develop a single unifying framework for the characterization and design of new composites. Consequently, there exists many approaches for

approximating the properties of ferroelectric composites[10], including asymptotic homogenization [11], mean field approaches[12], and laminate theory[13] to name a few.

In addition, work in the literature on augmenting the piezoelectric coefficients of ferroelectric composites typically focuses on amplifying the existing piezoelectric properties rather than changing the distribution of the properties[14][15]. This focus is likely driven by the desire for a high response out of the material when used in most practical applications, but for certain situations it may be desirable to also change the distribution of the piezoelectric properties of the material at hand. In this way, the resulting piezoelectric material property space could be densely populated from just a single material whose properties can be systematically estimated using one model rather than needing many different composites types and many different models to achieve the same outcome. To summarize, the three key motivators of this work are:

i) The dependency of ferroelectric material performance on crystallographic structure.
ii) A lack of a systematic and unifying framework for the design of new ferroelectric composites.
iii) The focus of contemporary work on augmenting existing ferroelectric property magnitudes rather than their distribution and the resulting limited piezoelectric property domain.

1.2. Hypothesis

With these motivations in mind, consider the sub-class of porous materials known as lattice materials. Lattice materials are made up of a unit cell pattern repeated in 3D space. The volume of research on lattice materials has increased in recent decades due to advancements in additive manufacturing that enable the manufacturing of complex geometries with ease[16]. Much work on tuning the materials properties of these materials through micro-architecture exists[16][17][18][19][20][21]. It has been shown that simply through adjustments in micro-architecture, the effective material properties of these lattice materials can be drastically different from the material that forms the lattice material itself [16][17][18].

The hypothesis of the present work arises from this observation. It is hypothesized that it may be possible to rationally design the performance of additively manufacturing ferroelectric lattice

materials independent of their crystalline structure and achieve a wide domain of ferroelectric properties combinations through micro-architecting of ferroelectric lattice materials.

1.3.Objective

The limitations in ferroelectric property tunability due to dependency on inherent crystalline structure and lack of a unifying design framework for existing composite ferroelectric materials motivates the present work. The objective of this work is to achieve rational design of ferroelectric lattice materials whose $\{d_{31}, d_{32}, d_{33},\}$ piezoelectric coefficients are tunable through structural design of lattice micro-architecture. Following the development of a design framework, application of ferroelectric structures as a multi-directional stress sensor is demonstrated.

1.4. Overview

The work begins with design methodology of ferroelectric lattices. The architectural design of these lattices begins with the unit cell. The plane angle is selected as the design parameter in this work and variations in this angle are used to generate new unit cell designs. Unit cells are tessellated in 3D space to form a lattice material. An analytical framework based upon a volume-averaging approach that allows for the rational design of ferroelectric lattice materials is developed. Following this, finite element computer simulations on unit cell and lattice models are performed to verify the analytically predicted piezoelectric coefficients. Finally, the piezoelectric properties of a few select lattices are verified experimentally by additively manufacturing the lattice materials and performing impact testing on the materials. A practical application of the lattice material is demonstrated in the form of a multi-directional stress sensor.

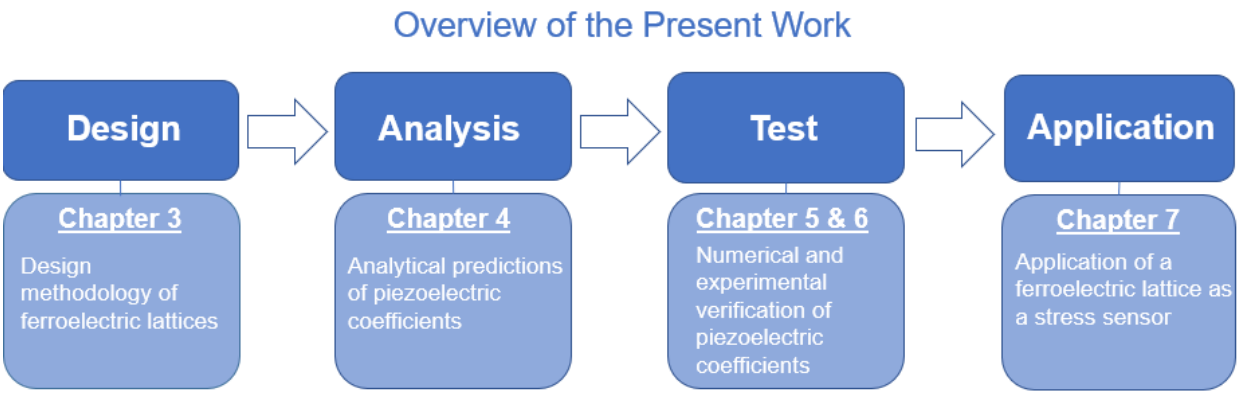

Figure 1. Overview of the present work.

Chapter 2: Background Information

The present work lies at the intersection of piezoelectricity, ferroelectric materials, and lattice materials. Background information in each of these areas is presented in this chapter.

2.1. The Piezoelectric Effect

Piezoelectricity is the characteristic of certain materials that exhibit a coupling between mechanical and electrical responses. This effect is a result of non-centrosymmetric crystalline structure[22]. Therefore, piezoelectricity only occurs in materials that belong to one of the twenty-one non-centric crystal classes[9]. This crystalline asymmetry can be observed in Fig. 2. in the perovskite lead zirconate titanate (PZT), a commonly used piezoelectric material from the 4mm crystallographic class. Fig. 3 depicts a polycrystalline piezoelectric material undergoing polarization due to an applied force. Initially, each molecule is electrically neutral in Fig. 3a. Application of force deforms the molecule and generates a dipole in Fig. 3b. In a large sample of the material, each molecule contributes a dipole, and the sum of these dipoles results in an overall polarization across the material in Fig. 3c.

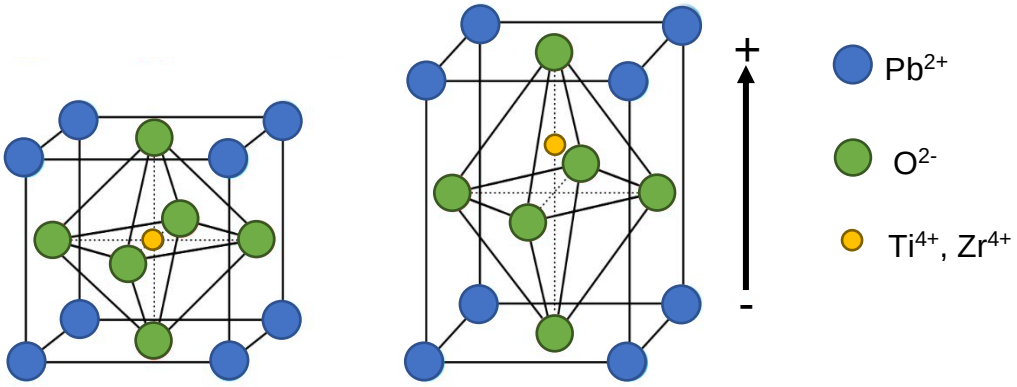

Figure 2. Perovskite structure of PZT. The displacement of the titanium due to stress or electric field results in the piezoelectric effect.

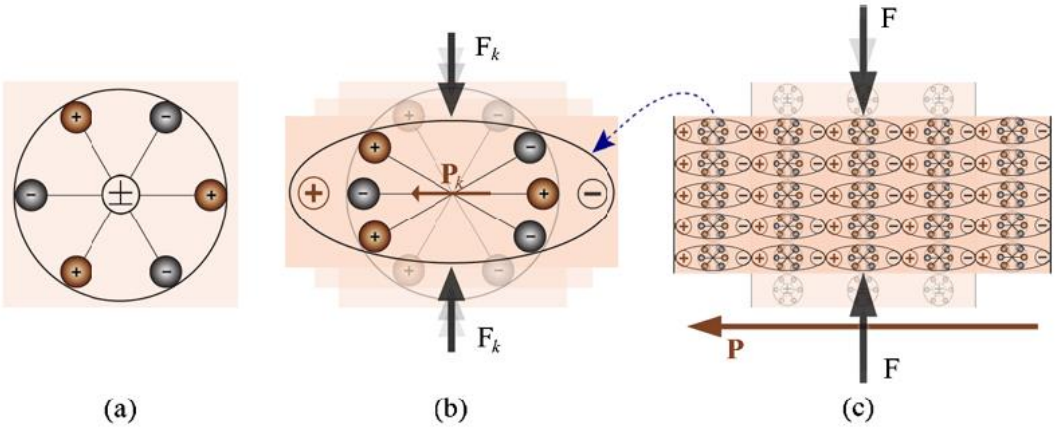

Figure 3. (a) Electrically neutral piezoelectric molecule. (b) Application of force deforms the geometry of the molecule and creates a dipole. (c) Resulting electric in a piezoelectric material from the sum of the polarization of the individual molecules[23].

The piezoelectric effect exhibits duality and is composed of the direct piezoelectric effect and the indirect piezoelectric effect. In the direct piezoelectric effect, a mechanical input results in an electrical response. In the indirect piezoelectric effect, an electrical input results in a mechanical response. A mechanical input or response can be either stress (σ) or strain (ξ). An electrical input or response can be either electric field (E) or electric displacement (D). These linear relationships are illustrated in the Heckmann diagram of Fig. 4.

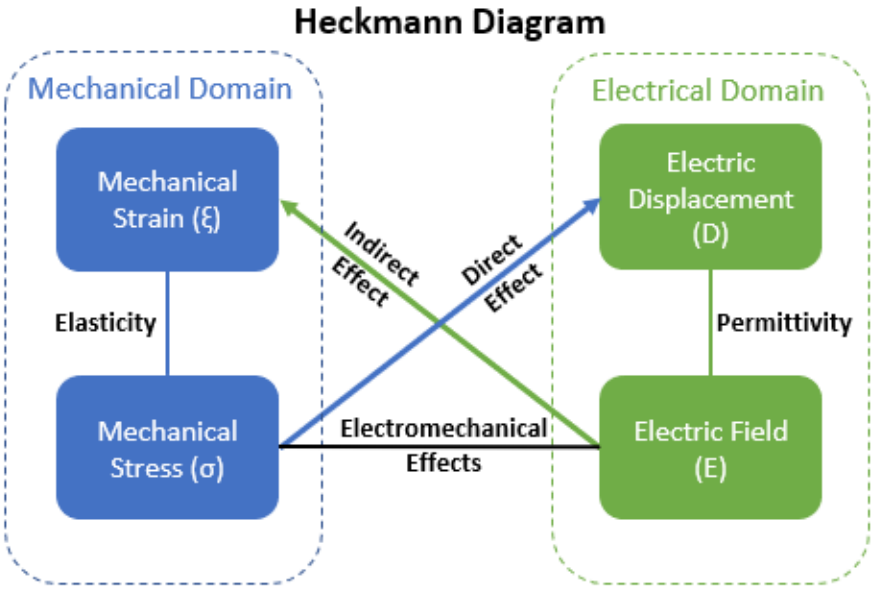

Figure 4. The Heckmann diagram shows the linear relationships between the mechanical and electrical variables of the piezoelectric effect[24].

2.2.1. Piezoelectric Coefficients

The piezoelectric coefficient is the ratio between mechanical input and electrical response or vice versa in the material. The coefficients quantify the piezoelectric performance of a material in different spatial directions and are assembled into a rank-three tensor. Voigt notation contracts tensor into a 3×6 or 6×3 matrix form for convenience[9].

Each piezoelectric coefficient has two subscripts. Take for instance the 4mm crystallographic class, which has five constants: $d_{31}, d_{32}, d_{33}, d_{15}$, and d_{24}. This particular set of direct piezoelectric coefficients are the ratio of electric displacement generated due to an applied stress. A matrix representation of the coefficient tensor is given in Eqn (1):

$$[d_{4mm}] = \begin{bmatrix} 0 & 0 & 0 & 0 & d_{15} & 0 \\ 0 & 0 & 0 & d_{24} & 0 & 0 \\ d_{31} & d_{32} & d_{33} & 0 & 0 & 0 \end{bmatrix} \quad (1)$$

The first subscript refers to the direction of the electric displacement while the second subscript refers to the direction of applied stress. Here 1, 2, and 3 correspond to the x-,y-, and z-directions and 4, 5, 6 and correspond to the yz-, xz-, and xy-planes respectively. It should be noted that for the 4mm crystalline class, $d_{31} = d_{32}$ and $d_{15} = d_{24}$, leaving only three independent coefficients. Fig. 5 illustrates the labeling convention for piezoelectric coefficients. In the present work, d_{31}, d_{32}, and d_{33} are selected as the parameters of interest and tuning of d_{24} and d_{15} are not considered.

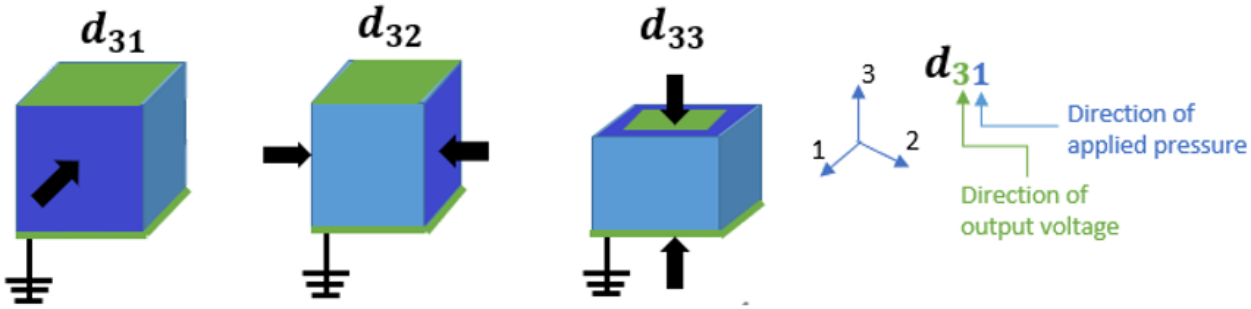

Figure 5. Labelling convention for piezoelectric coefficients.

The number of independent piezoelectric coefficients and their location within the tensor is determined by the crystallographic class of the piezoelectric material[32]. Piezoelectric performance is strongly dependent on crystalline anisotropy and therefore a non-zero piezoelectric coefficient in the tensor is the result of crystalline asymmetry for that particular crystallographic orientation. Conversely, a piezoelectric coefficient of zero indicates no piezoelectric effect because there is crystallographic symmetry for that orientation.

Tuning of these piezoelectric coefficients is possible. For crystalline ferroelectrics, domain engineering[6][25], doping[7][26], and thermal tuning[8][25] are common methods. For composite ferroelectrics, the methods are more diverse but to name a few, compositional grading[27], addition of piezoelectric particle inclusions[28], and fiber reinforcement[29], are such methods. Overall, the working principle behind methods for tuning piezoelectric coefficients in crystalline and composite ferroelectrics is modification of the structure of the material, either at the crystalline or micromechanics level. This reinforces the idea that piezoelectric performance is highly dependent on material structure.

2.2.2. Constitutive Piezoelectric Equations

The complete set of constitutive equations for the linear piezoelectric effect are derived from thermodynamic functions containing mechanical, electrical, and thermal arguments. The thermal arguments are often considered to be negligible and dropped, leaving only the two equations given in Eqn (2) and Eqn (3) containing the mechanical and electrical arguments.

$$\xi_p = s_{pq}^E \sigma_q + d_{fp} E_f \tag{2}$$

$$D_k = d_{kl} \sigma_l + \varepsilon_{kr}^\sigma E_r \tag{3}$$

These electromechanical variables are tensors of various rank and are summarized in Table 1. Voigt contraction is used to reduce the tensor rank of some variables.

Table 1. Summary of Variables in the Piezoelectric Constitutive Equations

Variable	*Property*	*Units*	*Full Tensor Rank*	*Voigt Contraction Rank*
ξ	Strain	$\frac{m}{m}$	2	1
s	Elastic compliance	$\frac{m^2}{N}$	4	2
σ	Stress	$\frac{N}{m^2}$	2	1
d	Piezoelectric coefficient	$\frac{pC}{N}$	3	2
E	Electric field	$\frac{V}{m}$	1	1
D	Electric displacement	$\frac{C}{m^2}$	1	1
ε	Dielectric permittivity	$\frac{F}{m}$	2	2

The direct and indirect piezoelectric effect can be observed in the constitutive equations. In Eqn (1), the indirect piezoelectric effect is contained within the second term of right-hand side, $d_{fp}E_f$, which relates the electric field contribution to the strain. In Eqn (2), the direct piezoelectric effect is contained within the first term on the right-hand side, $d_{kl}\sigma_l$, which relates the stress to the electric displacement.

The piezoelectric tensor 'd' is selected as the parameter of interest for this work but it should be noted that for each of the four possible combinations of mechanical and electric responses, there is a piezoelectric tensors that corresponds to each. Table 2 tabulates the tensors and their relations.

Table 2. Piezoelectric Tensor and Their Relations

Piezoelectric Tensor	*Relation*
d	Stress and electric displacement
g	Stress and electric field
h	Strain and electric field
e	Strain and electric displacement

2.2. Ferroelectric Materials

Ferroelectric materials are a sub-class of piezoelectric materials. In addition to possessing all the qualities of piezoelectric materials, ferroelectric materials are also capable of being poled[4]. Poling is the process of re-orienting and aligning the dipoles present in a material through application of a strong electric field. One such poling method is Corona poling, during which a material is poled by the strong electric field from an electrically charged needle[31]. Ferroelectrics exhibit outstanding electromechanical properties as a result of poling and are the most commonly used group of smart materials[9]. Applications include including sensors[1], precision actuators[2], active vibration dampers[3], medical imaging devices[4], and energy harvesters[5]. Ferroelectric materials can be further generally categorized into three groups: single domain ferroelectric crystals, ferroelectric ceramics, and ferroelectric composites. Fig. 6. shows the classification of the piezoelectric family.

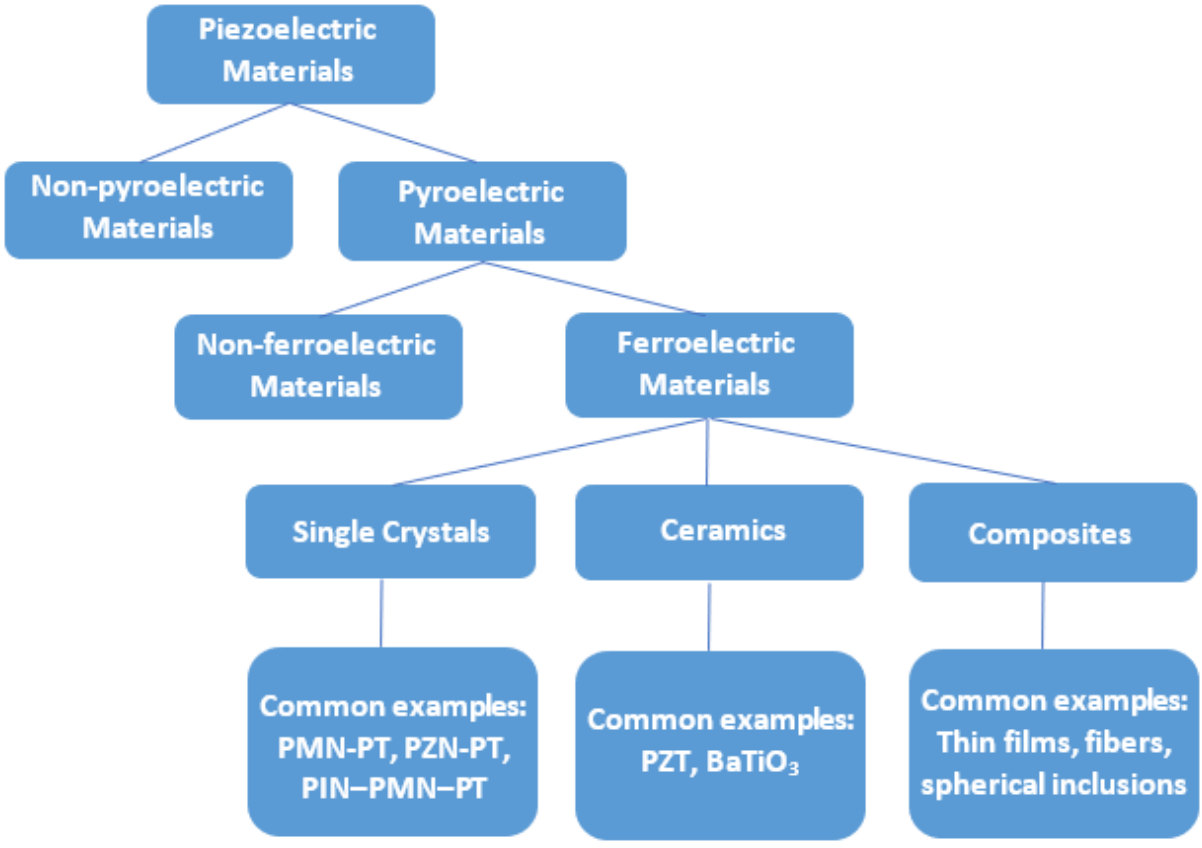

Figure 6. Classification of piezoelectric materials.

2.2.1. Effective Properties of Ferroelectric Composites

Out of the different types of ferroelectric materials, ferroelectric composites are the focus of this work. Ferroelectric composites are composed of at least two or more phases and the properties of the overall material is the resultant of these phases and their interactions. Therefore, the overall properties of the composite are different from its individual components and a set of effective material properties are typically used to characterize the composite. An effective medium approximation is the general term for any modeling method that estimates these effective material properties. Some common effective medium approaches are the effective medium method[32], the effective field method[32], the dilute solution[33][34], the differential scheme[35], and conditional moments method[36]. Out of these, the effective field method is one of the most widely used and has been demonstrated to be a reliable method for calculating effective properties[32][37][38] [33]. The effective field method is based off of the Mori-Tanaka method and uses eigenstrains to calculate an average stress in the material and derives other material properties from this stress[32].

While there are many approaches to obtaining effective properties of the material, the working principle behind each of them is to take the individual contributions of each phase and the interactions between phases to get some overall approximate value. This concept is later used in the present work to develop a volume-averaging method of calculating effective piezoelectric coefficients in the lattice.

2.3. Lattice Materials

Porous materials have been studied for hundreds of years, but interest in its subset of lattice materials have increased in most recent decades due to the accessibility of creating complex geometries enabled by additive manufacturing[39][40]. A lattice material is a material that is composed of a repeating geometric pattern that can be tessellated in 3D space; this repeated pattern can be considered as the “unit cell” for the lattice material, analogous to the atomic unit cell concept used in chemistry or materials science. Lattice materials have the advantaged of controlled porosity over foams, whose porosity is stochastic. As a result, the properties of lattice materials can generally be better characterized analytical than those of a foam.

Just as for composite materials, a set of effective materials properties is used to characterize the lattice material. Interestingly, these effective material properties can be tuned through simply changing the geometry of the lattice unit cells[41][42][17]; this process is known as "architecting." Yang et al demonstrated tunability of Poisson's ratio, normalized modulus, and normalized compressive strength in lattice materials[41]. Ahmadi et al studied the behavior of diamond lattice biomaterials as a function of relative density[42]. Sometimes the properties of these lattice materials are found to exceed those of the base material from which they are made from when comparing the density normalized properties of the materials. For instance, Zheng et al used projection microstereolithography and nancoscale coating to create ultrastiff microlattice materials[17]. As observed in piezoelectric materials, there appears to be a strong structure-property dependency in lattice materials as well. The difference lies in the scale at which the structure-dependency exists. Rather than at the crystalline level as in piezoelectric materials, the micro-scale structure in lattice materials strongly affects their effective properties.

This interesting observation forms the basis of the hypothesis of this work. It is hypothesized that the piezoelectric coefficients of a lattice ferroelectric material can tuned and rationally designed through mirco-architecting of the lattice structure rather than modification of the crystalline structure. Thus, the difference in approach between this work and traditional crystalline ferroelectric material augmentation lies at the scale at which the tuning is performed. That is, at the micro-scale rather than the crystalline scale.

2.4. Ferroelectric Lattice Materials

A literature review reveals that work in the area of piezoelectric or ferroelectric lattice materials has been done by several groups. Iyer et al. studied the electromechanical response of 2D piezoelectric honeycomb structures with varying types of porosity[43]. Bosse et al. studied the effect of foam shape on effective electromechanical properties in 3D cubic foams[44]. Shimada et al. studied the ferroelectric and ferrotoroidic polarizations in 2D lattice materials[45]. Shi et al. studied the effects of pore geometry on thermoelectromechanical properties in 3D cubic foams[46]. However, these works only study 2D lattices or simple 3D lattice designs that have been well characterized in the literature. The literature seems to lack work in which an over-arching framework for the design and analysis of new, complex 3D ferroelectric lattice materials is

developed. Thus, in the present work, such a framework is presented and forms a key contribution of the work.

Chapter 3: Framework for Lattice Design

From chemistry, a unit cell is defined as the smallest group of atoms that capture the behavior of a material and can be repeated in 3D space to form the structure of the material. Similarly, for lattice materials, a unit cell can be defined as the smallest volume that can be patterned to generate the lattice. Since the unit cell is the primitive unit of a lattice material and fully captures the geometry of the overall lattice, it makes sense to begin the design process with the unit cell.

For the present work, the design methodology behind generating micro-architected ferroelectric lattice materials begins with the two-dimensional projection pattern of the unit cell and variation of the plane angle in the unit cell. Transition from the two-dimensional design to a three-dimensional design is achieved through the screw angle. The resulting three-dimensional body can then be tessellated into a lattice to create a lattice material. An overview of this process is presented in Fig. 7.

Figure 7. High-level overview of the ferroelectric lattice material design process.

3.1. Two-Dimensional Design Space

The objective of the design methodology in the present work is to establish a framework that can be broadly applied to generate a variety of three-dimensional ferroelectric lattice material designs. Although the final architected lattice materials are three-dimensional, the design process begins in the two-dimensional space. Starting from two-dimensional space constrains the design space and makes the overall process more intuitive. In general, it is much easier for humans to imagine a complex 2D shape than a complex 3D shape; consider an analogy using shadow puppets shown in Fig. 8. To create a shadow puppet, the individual would typically not be looking at the complex 3D configuration of the hand itself, but rather on the resulting 2D shadow that is casted. For the

simple designs considered in this work it may seem less cumbersome to simply start with a three-dimensional design. However, since a key objective of this work is to establish a design framework for which even very complicated lattice designs can be realized, it becomes critical to use the two-dimensional designs as a bridge to the three-dimensional lattice materials.

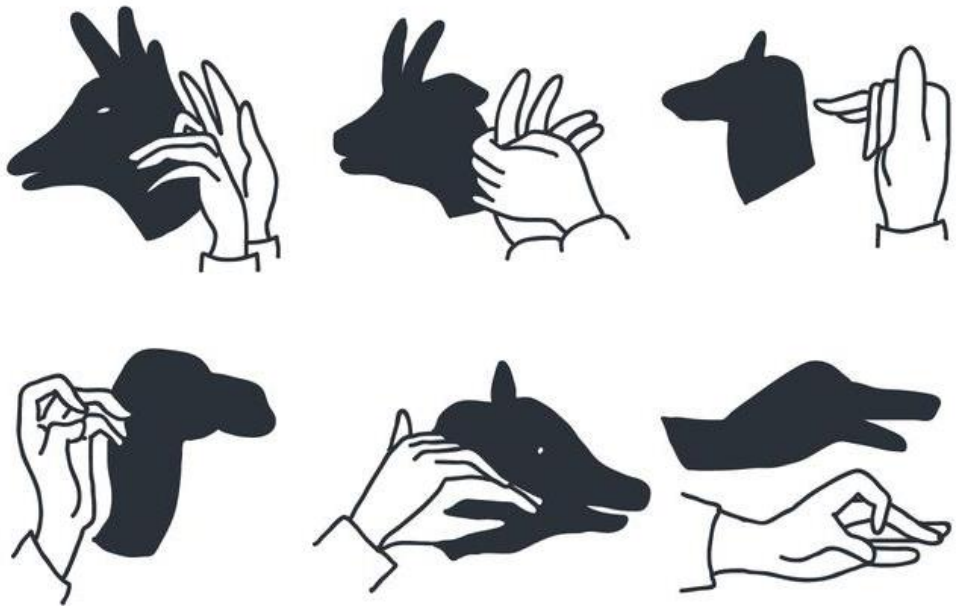

Figure 8. Hand shadow puppets and their 2D projections[48].

Two-dimensional auxetic, square, and honeycomb patterns are selected as the unit cell patterns in the present work because these structures are already well-studied in the literature and have an existing basis for their analysis[14][48][49][50]. The projection pattern of the unit cell is characterized by the strut radius (r), vertical strut length (l_v), the angled strut length (l_a), and the plane angle (Θ_{plane}). Note that plane angles less than 90° give an auxetic pattern, plane angles equal to 90° give a square pattern, while plane angles greater than 90° give a honeycomb pattern. This relationship is illustrated in Fig. 9. Thus, the plane angle provides a convenient link between the different unit cell designs and is selected as the design parameter for the present work Though the plane angle was chosen due it being a convenient link between different types structures, it should be noted that any other geometric property such as strut radius, strut length, or nodal connectivity could have been chosen as well. The proposed design method makes it possible to generate an

infinite number of 2D unit cell designs, from simple well-studied structures like the auxetic, cubic, and honeycomb, to very complex designs that have yet to be discovered.

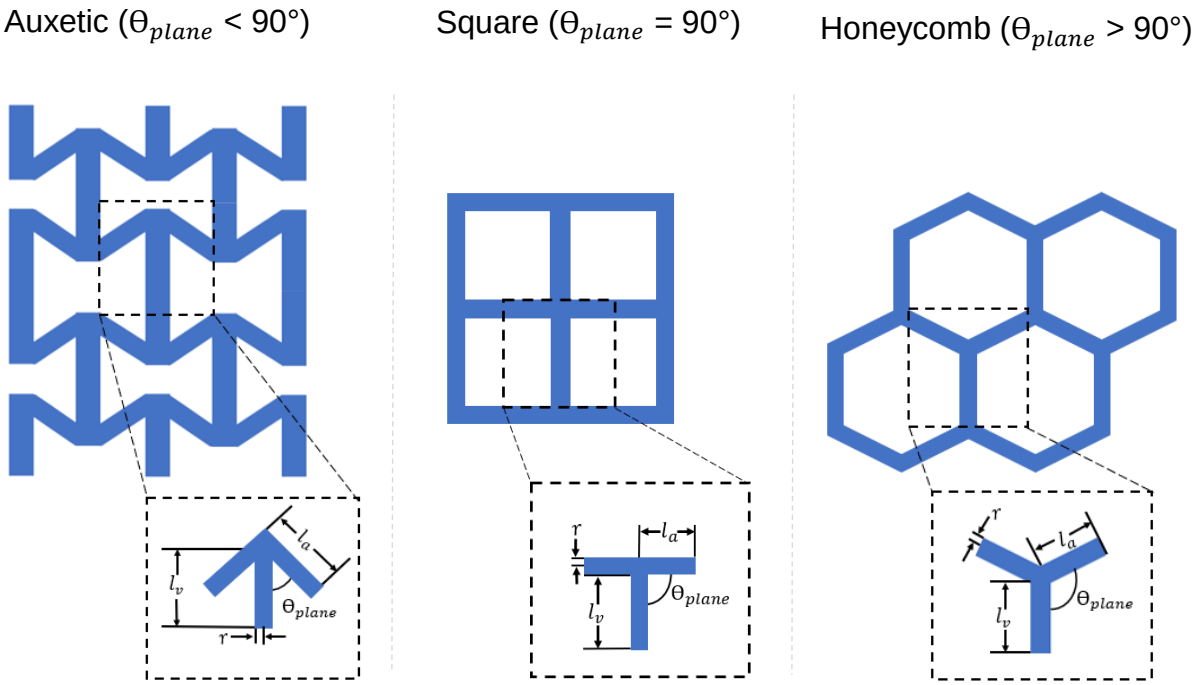

Figure 9. Two-dimensional projection pattern parameters.

3.2. Transition to Three-Dimensional Space

Before transitioning into three-dimensional space, an alternate two-dimensional pattern derived from the previous pattern is used. While the previously presented patterns are simpler because they contain less struts, an alternative representation of the unit cell is necessary because later periodic boundary conditions used in finite element analysis require geometric symmetry. The alternative pattern for the honeycomb structure is shown in Fig. 10. but alternative patterns for the auxetic and square structure can be derived similarly.

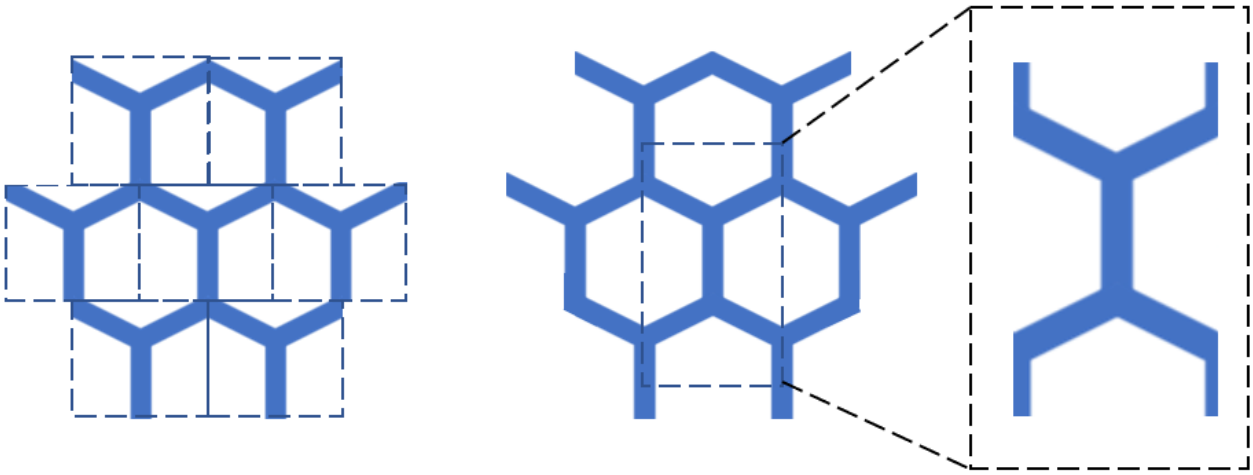

Figure 10. Alternative unit cell representation used for finite element analysis due to geometry symmetry.

The two-dimensional projection pattern is linked to the final three-dimensional unit cell by the screw angle, Θ_{sc}. The screw angle is defined as the angle between the plane of the projection pattern and the rotated plane through which the center line of the angled struts lie. The 3D unit cell also contains a new parameter called the space angle (Θ_s). The space angle lies in the rotated plane and is the angle between the angled struts the vertical strut. Note the space angle differs from the plane angle but these two angles can be related by trigonometric relationships. The designs considered in this work have two rotated planes with $\Theta_{sc} = 45°$ to create a total of nine vertical struts in each unit cell, but any number of planes could be used to give more struts. In Fig. 11, a unit cell with two rotated planes of $\Theta_{sc} = 45°$, $\Theta_p = 120°$, and $\Theta_s = 109°$ is shown. By varying the plane angle, we can obtain different unit cells designs, shown in Fig. 12. It should be noted that for the present work the screw angle was chosen as the link between the 2D pattern to the 3D unit cell due to its simplicity, but another means could just as easily been chosen to be the design parameter. This gives a lot of freedom in generating the 3D unit cell and its resulting geometries.

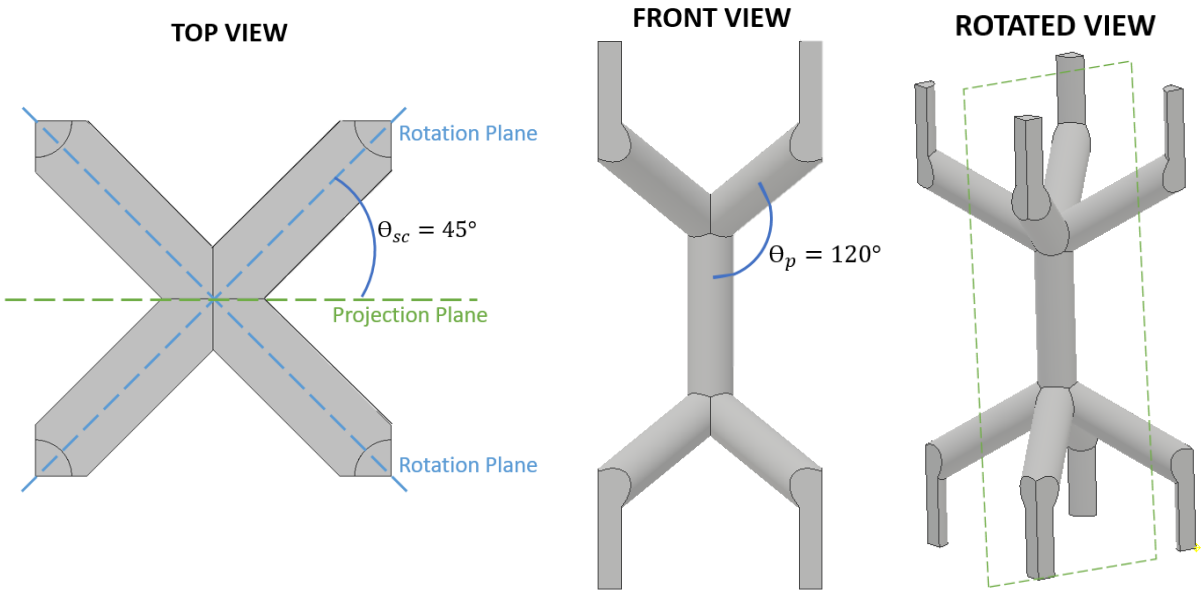

Figure 11. Schematic of the various design angles within the model.

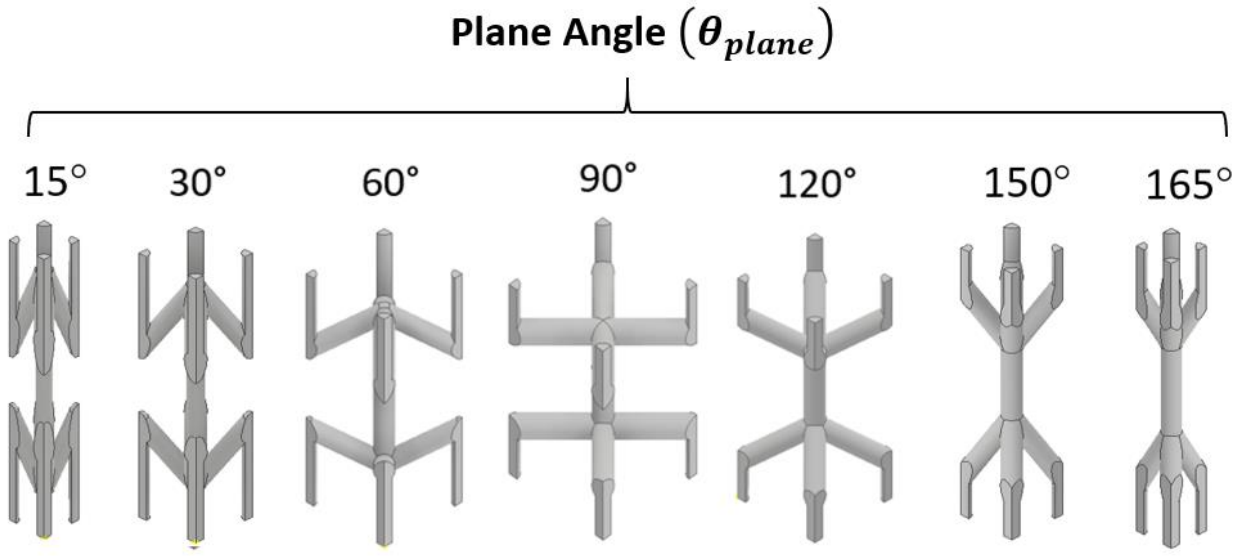

Figure 12. CAD models of the unit cells used in this study. The 15°, 30°, and 60° unit cells are auxetic. The 90° unit cell is square. The 120°, 150°, 165° unit cells are honeycomb.

3.3. Transition to a 3D Lattice

Finally, tessellation of the unit cells yields a lattice material. Different unit cells give different lattice materials. In the present work, unit cell designs with plane angle ranging from 15° to 165° are studied, resulting in seven unique lattice materials. Fig. 13. shows each of the lattice materials.

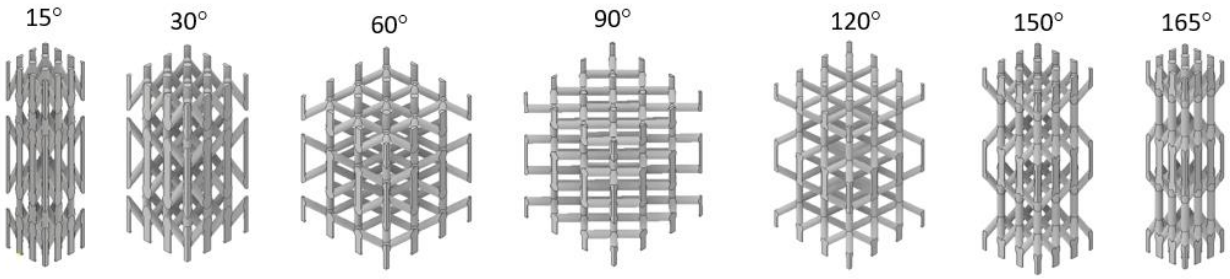

Figure 13. Tessellation of each unit cell forms a unique three-dimensional lattice material.

Chapter 4: Analytical Modeling

Following the design of the ferroelectric lattice materials, analytical calculations through a volume-averaging method are performed in order to estimate the piezoelectric coefficients of different lattice designs. While the overall geometry of the unit cells are complicated, the unit cells can be broken down into the individual struts that make them up and approximated as beams. Thus, a greatly simplified analysis can be performed on the individual beams and their contributions can be summed to obtain that of the overall unit cell. The method presented in this work was developed by Cui et al.[51]. The idea behind this method stems from several works in the literature that calculate the effective mechanical properties of lattice materials using approaches based off beam models. Yang et al. used the Timoshenko beam model to calculate properties of a 3D re-entrant honeycomb auxetic structure[33]. Deshpande et al. analytically calculated the effective properties of octet-truss lattice materials using the Timoshenko beam model[52]. Dong et al. used a DFA model after Deshpande et al[52] to model the response of octet truss lattice structures[53].

In the present work, the Euler beam model and nodal force equilibrium are used to obtain local stresses in individual struts. The local stresses are then transformed into the global stress. Piezoelectric behavior in each strut is then incorporated into the model through the relationship between global stress and local electric displacement in each strut. Finally, the piezoelectric contribution of each strut is summed and volume averaged to obtain the effective piezoelectric coefficient of the unit cell. General forms of equations that can be applied to any ferroelectric lattice structure are derived. Following this, specific equations for the structures considered in this work are derived and are applied to predict the piezoelectric coefficients.

4.1.Volume Averaging Scheme

The effective piezoelectric coefficients of each lattice material are calculated through a homogenization scheme of the electric displacement in each strut within the unit cell. The electric displacement in the strut arises from the stress applied on the unit cell. The relationship between electric displacement (D_n) and applied stress (σ_{KL}) is given in Eqn (4) by

$$D_n = d_{nKL}\sigma_{KL} \tag{4}$$

Where d_{nKL} is the direct piezoelectric coefficient, and n, K, L = 1, 2, 3 in the global 1-2-3 coordinate system. The electric displacement and stress in each strut are summed and normalized by the cubic volume occupied by the unit cell (V), giving the volume averaged values of electric displacement and stress of the overall unit cell in Eqn (5) as

$$\begin{cases} D_n = \frac{1}{V}\sum_{i=1}^{N}\int_{V_i} D_n^{(i)}\, dV_i \\ \sigma_{KL} = \frac{1}{V}\sum_{i=1}^{N}\int_{V_i} \delta_{Kk}\delta_{Ll}\sigma_{kl}^{(i)}\, dV_i \end{cases} \tag{5}$$

Where $k, l = 1,2,3$, and δ_{Kk}, δ_{Ll} are Kronecker delta operators. For the local stress of each strut ($\sigma_{kl}^{(i)}$), a local coordinate system denoted by 1'-2'-3' is used. A stress transformation is needed in order to transform the local stress into stress in the global coordinate system in Eqn (6) and Eqn (7)

$$\sigma_{kl}^{(i)} = N_{kp}^{(i)}\sigma_{pq}^{(i)}\left(N_{ql}^{(i)}\right)^T \tag{6}$$

$$N^{(i)} = \begin{bmatrix} \cos\theta_2 & 0 & \sin\theta_2 \\ 0 & 1 & 0 \\ \sin\theta_2 & 0 & -\cos\theta_2 \end{bmatrix}\begin{bmatrix} 1 & 0 & 0 \\ 0 & \cos\theta_1 & \sin\theta_1 \\ 0 & \sin\theta_1 & -\cos\theta_1 \end{bmatrix}\begin{bmatrix} \cos\theta_3 & \sin\theta_3 & 0 \\ \sin\theta_3 & -\cos\theta_3 & 0 \\ 0 & 0 & 1 \end{bmatrix} \tag{7}$$

Where N is the transformation matrix composed of Euler angles θ_1, θ_2 and θ_3 and the indices p, q = 1', 2', 3'. Rearranging Eqn. (4) and substitution gives the effective piezoelectric coefficients in Eqn (8) as

$$d_{nKL} = \frac{D_n}{\sigma_{KL}} = \frac{\sum_{i=1}^{N} A_i|L_i| d_{nkl} N_{kp}^{(i)}\sigma_{pq}^{(i)}N_{ql}^{(i)}}{\sum_{i=1}^{N} A_i|L_i|\delta_{kK}\delta_{lL}N_{kp}^{(i)}\sigma_{pq}^{(i)}N_{ql}^{(i)}} = \frac{\sum_{i=1}^{N} d_{nkl}\, N_{kp}^{(i)}\sigma_{pq}^{(i)}N_{ql}^{(i)}}{\sum_{i=1}^{N}\delta_{kK}\delta_{lL}N_{kp}^{(i)}\sigma_{pq}^{(i)}N_{ql}^{(i)}} \tag{8}$$

Where A_i and $|L_i|$ are the cross-sectional area and length of the struts. Here, we assume all struts have the same cross-sectional area and strut length. Thus, the effective piezoelectric coefficients

of the unit cell, and consequently the lattice material, can be calculated in this fashion. This method can be applied generally to any lattice design.

Following the derivation of a general solution that can be applied to any unit cell design, specific equations for the unit cell designs considered in the present work are derived. Geometric parameters of the unit cell are shown in Fig. 14. Note that the unit cell contains only two unique strut types, angled and vertical, simplifying the calculations. These struts are labeled “a” and “b” respectively in Fig. 14.

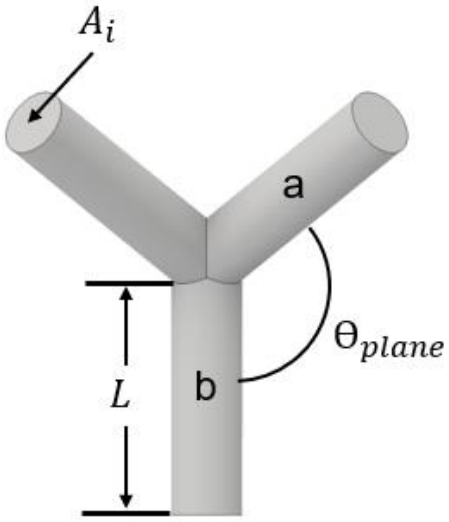

Figure 14. Unit cell parameters.

The stress transformation matrix for the two strut types are given below in Eqn (9). Note $\Theta_3 = \Theta_{sc}$ and $\Theta_4 = \arctan\left(\sqrt{2}tan\left(\Theta_{plane} - 90\right)\right)$.

$$\begin{bmatrix} N_{11}^a & N_{12}^a & N_{13}^a \\ N_{21}^a & N_{22}^a & N_{23}^a \\ N_{31}^a & N_{32}^a & N_{33}^a \end{bmatrix} = \begin{bmatrix} cos\Theta_3 cos\Theta_4 & -sin\Theta_3 & -cos\Theta_3 sin\Theta_4 \\ cos\Theta_3 cos\Theta_4 & cos\Theta_3 & -sin\Theta_3 sin\Theta_4 \\ sin\Theta_4 & 0 & cos\Theta_4 \end{bmatrix}$$
$$\begin{bmatrix} N_{11}^b & N_{12}^b & N_{13}^b \\ N_{21}^b & N_{22}^b & N_{23}^b \\ N_{31}^b & N_{32}^b & N_{33}^b \end{bmatrix} = \begin{bmatrix} 0 & 0 & 1 \\ 0 & 1 & 0 \\ -1 & 0 & 0 \end{bmatrix} \quad (9)$$

Substituting Eqn (5), the effective electric displacement and stress in Eqn (10) become

$$D_3^{eff} = \frac{1}{V}\{d_{31}\ d_{32}\ d_{33}\}\left(4A_1|L_1|\begin{Bmatrix}\sigma_{11}^1\\ \sigma_{22}^1\\ \sigma_{33}^1\end{Bmatrix} + A_5|L_5|\begin{Bmatrix}\sigma_{11}^5\\ \sigma_{22}^5\\ \sigma_{33}^5\end{Bmatrix}\right) \tag{10}$$

$$\sigma_{33} = \frac{1}{V}(4A_1|L_1|\sigma_{33}^1 + A_5|L_5|\sigma_{33}^5) \tag{11}$$

From force equilibrium, the force on the unit cell (F) is given in Eqn (12) as

$$F = 4\sigma L^2 \sin^2\Theta_3\, cos^2\Theta_4 \tag{12}$$

From the force equilibrium, the local stress for each strut type are found in Eqn (13) and Eqn (14) to be

$$\sigma_{pq}^{(a)} = \frac{\sigma L_a^2}{A_a}\begin{bmatrix} sin^2\Theta_3 cos^2\Theta_4 sin\Theta_4 & 0 & sin^2\Theta_3 cos^3\Theta_4 \\ 0 & 0 & 0 \\ sin^2\Theta_3 cos^3\Theta_4 & 0 & 0 \end{bmatrix} \tag{13}$$

$$\sigma_{pq}^{(b)} = \frac{4\sigma L_b^2}{A_b}\begin{bmatrix} sin^2\Theta_3 cos^2\Theta_4 & 0 & sin^2\Theta_3 \\ 0 & 0 & 0 \\ 0 & 0 & 0 \end{bmatrix} \tag{14}$$

Substitution of these derivations in Eqn (8) gives the following expressions for the effective piezoelectric coefficients of the unit cells presented in this work in Eqn (15) and Eqn (16) as

$$d_{31}^{eff} = d_{32}^{eff} = \frac{-cos^3\Theta_3 cos^2\Theta_4 sin\Theta_4 d_{31} - sin^2\Theta_3 cos\Theta_3 cos^2\Theta_4 sin\Theta_4 d_{32} + cos\Theta_3 sin\Theta_4(1+cos^2\Theta_4)d_{33}}{2sin\Theta_3\cos\Theta_4} \tag{15}$$

$$d_{33}^{eff} = \frac{-cos^2\Theta_3 cos^2\Theta_4 sin\Theta_4 d_{31} - sin^2\Theta_3 cos^2\Theta_4 sin\Theta_4 d_{32} + (sin\Theta_4(1+cos^2\Theta_4)+1)d_{33}}{2+2sin\Theta_4} \tag{16}$$

Note $d_{31}^{eff} = d_{32}^{eff}$ due to unit cell symmetry in these directions for the designs considered in the current work, but non-symmetric designs may be used as well to yield unique values for d_{31}^{eff}, d_{32}^{eff}, and d_{33}^{eff}.

4.1.1. Normalized Piezoelectric coefficients

Since changing the distribution of the piezoelectric coefficients is of interest in this work rather than changing magnitude of the coefficients, a piezoelectric coefficient vector is defined in this work. The vector is composed of the normalized piezoelectric coefficients $\vec{d} = \langle d_{31}^*, d_{32}^*, d_{33}^* \rangle$. Note that the normalized piezoelectric coefficient, d_{31}^*, differs from the effective coefficient, d_{31}^{eff}, calculated in the previous section. The normalized piezoelectric coefficients are obtained by normalizing each coefficient by the magnitude of the overall vector. The normalized piezoelectric coefficients $\{d_{31}^*, d_{32}^*, d_{33}^*\}$ are given by Eqn (17) as

$$d_{31}^* = \frac{d_{31}^{eff}}{\sqrt{\left(d_{31}^{eff}\right)^2 + \left(d_{32}^{eff}\right)^2 + \left(d_{33}^{eff}\right)^2}}$$
$$d_{32}^* = \frac{d_{32}^{eff}}{\sqrt{\left(d_{31}^{eff}\right)^2 + \left(d_{32}^{eff}\right)^2 + \left(d_{33}^{eff}\right)^2}} \quad (17)$$
$$d_{33}^* = \frac{d_{33}^{eff}}{\sqrt{\left(d_{31}^{eff}\right)^2 + \left(d_{32}^{eff}\right)^2 + \left(d_{33}^{eff}\right)^2}}$$

The purpose of this normalization process is to further facilitate comparison of piezoelectric coefficient distribution. By normalizing the coefficients, a unitless vector space of d_{33}^* versus d_{31}^* is obtained. The piezoelectric coefficients reported in this work will be the normalized piezoelectric coefficients from this point forward unless specified otherwise.

4.2. Analytical Results and Discussion

The analytically estimated piezoelectric coefficients for each of the unit cell designs with plane angles ranging from 15° to 165° are summarized in Table 3. Fig. 15. plots the dimensionless,

normalized piezoelectric coefficients (d_{31}^* and d_{33}^*) versus plane angle (Θ_{plane}). Based off the results, for $\Theta_{\boldsymbol{plane}}$ less than some value between 90° and 120°, the d_{31}^* coefficient is negative. Above this value, the d_{31}^* coefficient is positive. The d_{33}^* coefficient appears to peak in magnitude at approximately 90° and tapers off as it approaches very small or large angles. This coefficient seems to always be positive as well.

Table 3. Analytically Calculated Piezoelectric Coefficients[51]

Plane Angle ($\Theta_{\boldsymbol{plane}}$)	**Normalized Piezoelectric Coefficient ($\boldsymbol{d_{31}^*}$)**	**Normalized Piezoelectric Coefficient ($\boldsymbol{d_{33}^*}$)**
15°	-0.69	0.19
30°	-0.68	0.27
60°	-0.46	0.76
90°	-0.28	0.92
120°	0.48	0.73
150°	0.64	0.43
165°	0.69	0.24

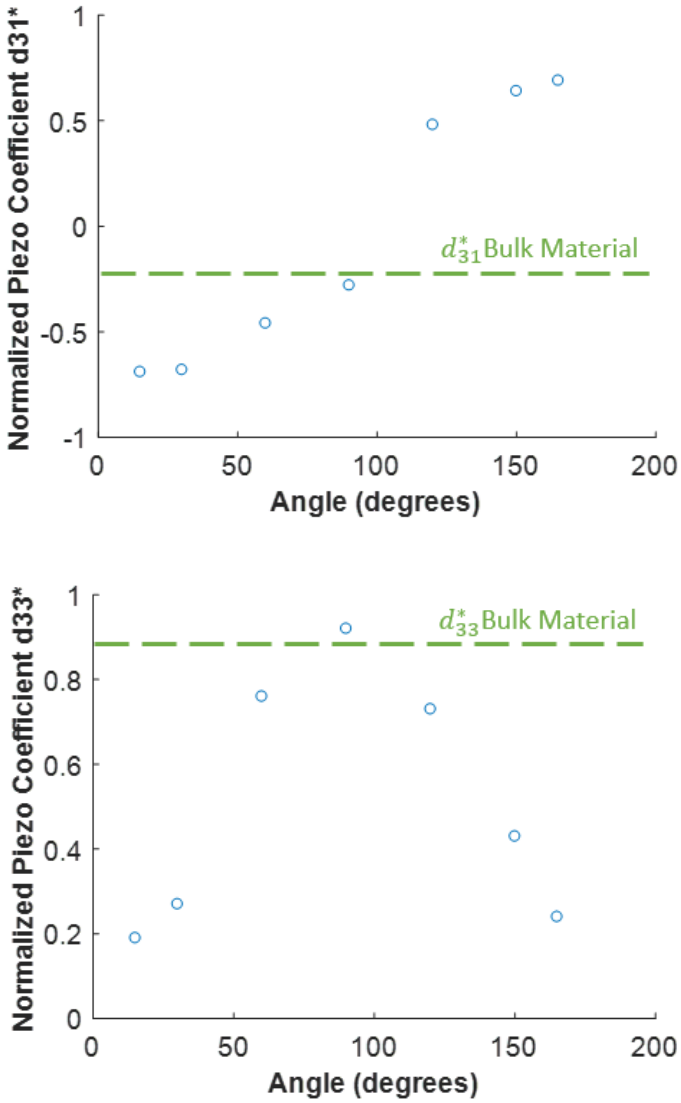

Figure 15. (Top) Plot of the normalized piezoelectric coefficient (d31*) versus unit cell plane angle. (Bottom) Plot of the normalized piezoelectric coefficient (d33*) versus unit cell plane angle

A plot of the unitless $d_{31}^*$and d_{33}^* vector space is shown in Fig. 16. Interestingly, it appears that unit cells with supplementary angles, i.e. 60° and 120°, have approximately the same magnitude but opposite signs for d_{31}^*. Therefore, it appears that it is possible to completely change the direction of material's response. In contrast, supplementary angles have approximately both the same magnitude and sign for d_{33}^*. It should be noted that the red star in the figure represents the piezoelectric vector of the base material that makes up each of the lattice materials. Therefore, the analytical results predict that it is possible to transform a single base material to multiple lattice materials with their own unique set of piezoelectric coefficients. As predicted in the hypothesis,

the normalized piezoelectric coefficients change as the plane angle of the unit cell angle is changed. In the following chapter, finite element simulation is used to provide another set of predicted piezoelectric coefficients. These results will be compared with the analytical predictions.

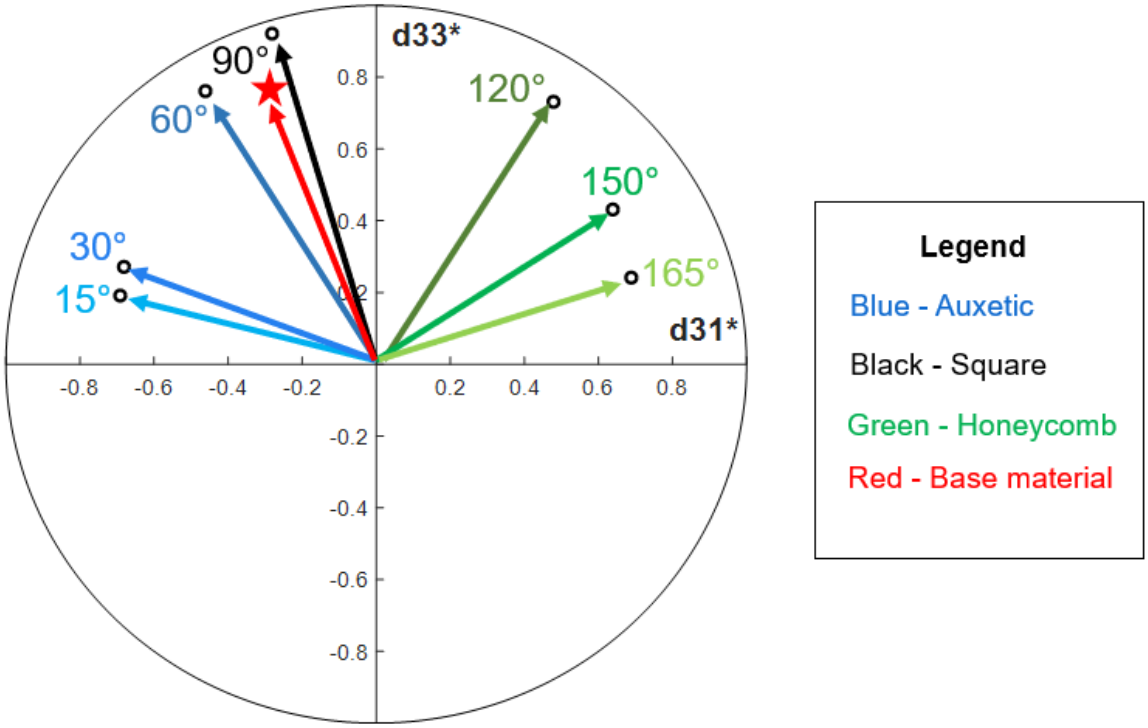

Figure 16. The dimensionless d31* and d33* vector space.

Chapter 5: Numerical Modeling

The purpose of this section is to use numerical modeling to provide verification of the analytical framework. A verified analytical framework would enable the rational design of ferroelectric lattice materials with tunable piezoelectric coefficients through micro-architecture. Numerical modeling of the lattice designs is performed using Abaqus 6.14 finite element software. A unit cell model with periodic boundary conditions approximating that of an infinite lattice is developed. The unit cell model results and post-processing method are verified through a simple cubic model. Following this, a lattice model is created to verify that the periodic boundary conditions are capable of capturing the behavior of an infinite lattice. Mesh convergence of the lattice model is verified.

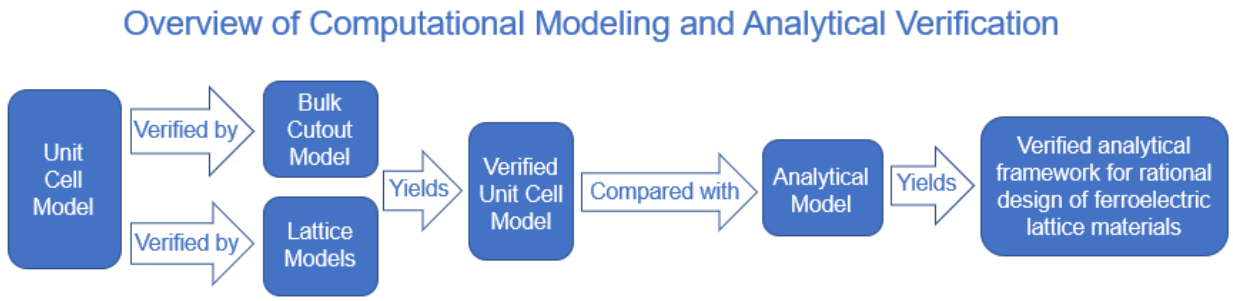

Figure 17. Overview of numerical models.

5.1. Unit Cell Model

The numerical analysis begins with the unit cell since it serves as the primitive unit of the lattice material and its smaller geometry saves numerical time. CAD models of each unit cell design were created in Autodesk Inventor 2017, a commercial CAD package, and then imported into ABAQUS 6.14 finite element software for analysis. A PZT composite that is capable of being additively manufacturing was used as the base material for the model. This material is the same material used in the previous analytical calculations. The electrical and mechanical properties of this material were experimentally measured and are summarized in Table 4 and Table 5. Tetrahedral piezoelectric elements (C3D10E) were used to mesh the model

Table 4. Electrical properties of the PZT composite

Electrical Property	Value
Dielectric constant (ε)	$\varepsilon_{11} = \varepsilon_{22} = 2.6 \times 10^{-10} \frac{F}{m}$ $\varepsilon_{33} = 1.1 \times 10^{-10} \frac{F}{m}$
Piezoelectric coefficient (d)	$d_{31} = d_{32} = -1.5 \times 10^{-11} \frac{m}{V}$ $d_{33} = 5.2 \times 10^{-11} \frac{m}{V}$ $d_{15} = d_{24} = 7.0 \times 10^{-11} \frac{m}{V}$

Table 5. Mechanical properties of the PZT composite

Mechanical Property	Value
Density (ρ)	$\rho = 1360 \frac{kg}{m^3}$
Young's Modulus (E)	$E = 554\ MPa$
Poisson's Ratio (ν)	$\nu = 0.4$

Periodic boundary conditions were used in order to capture behavior of an infinite lattice material by enforcing the same strain at corresponding positions on parallel surfaces using constraint equations. Wu et al used this approach and found it advantageous for reducing numerical time significantly[54], which is highly desirable in the present work. Eqn (18) shows the generic formula for the constraint equations, where p^{m1} and p^{m2} are the degrees of freedom of the master nodes and p_i^{s1} and p_i^{s2} are the i^{th} slave nodes.

$$p^{m1} - p_i^{s1} - (p^{m2} - p_i^{s2}) = 0 \tag{18}$$

The degrees of freedom on each node are displacement in the 1-, 2-, and 3-directions and electrical potential (9 in ABAQUS). The electric potential at the bottom 3-face was constrained to be zero in order to ground the unit cell. A pressure load was applied to the flat faces perpendicular to the 1-direction and 3-direction independently in order to measure the piezoelectric coefficients d_{31} and d_{33}. Recall that $d_{31} = d_{32}$ for the designs considered in this work due to their symmetric in the 1- and 2- directions.

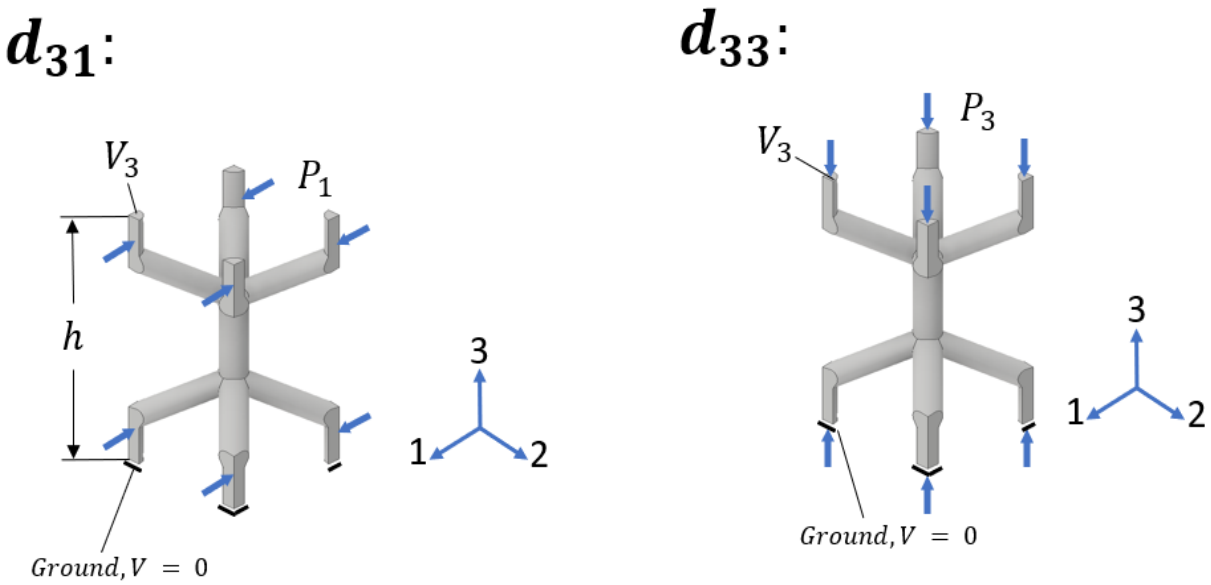

Figure 18. Model schematic for finite element simulation of d31* and d33*.

Simulation results were post-processed and piezoelectric coefficients were extracted. To achieve this, the electric field (E_f) of the unit cell was calculated using Equation (19), where V is the average voltage measured at the top of the unit cell and h is the height of the model. In order to calculate the piezoelectric charge coefficient (d), the piezoelectric voltage coefficient (g) is first calculated because the variables needed to calculate the piezoelectric voltage coefficient can be directly extracted from Abaqus. The voltage coefficient is calculated using the electric field (E_f) and applied stress (σ_i) in Equation (20). The piezoelectric voltage coefficients are related to the piezoelectric charge coefficients through the dielectric permittivity of the material (ε_{ii}) in Equation (21). The dielectric constant of the unit cell is calculated using the relative density of the lattice and the permittivity of the base material for a specific direction (i.e., ε_{33}).

$$E_f = \frac{V}{h_f} \tag{19}$$

$$\{g_{fp}\} = \begin{Bmatrix} g_{31} \\ g_{32} \\ g_{33} \end{Bmatrix} = \frac{E_f}{\sigma_p} \quad \left(\frac{V/m}{N/m^2}\right) \tag{20}$$

$$\{d_{fq}\} = \begin{Bmatrix} d_{31} \\ d_{32} \\ d_{33} \end{Bmatrix} = g_{fp}\varepsilon_{pq} \quad \left(\frac{V \cdot m}{N}\right)\left(\frac{F}{m}\right) \; for \; q = 1,\ 2,\ 3 \tag{21}$$

5.2. Unit Cell Model and Post-Processing Method Verification

A bulk material test was performed to verify results from the unit cell model and the post-processing method for obtaining the piezoelectric coefficients. It was hypothesized that if the finite element model is in fact reliable, the calculated piezoelectric coefficients should match that of the defined material properties and those predicted from the analytical method. The model consists of a solid rectangular block of the PZT composite material with dimensions of 1 m × 1 m × 2 m. Periodic boundary conditions are applied, and the same boundary conditions from the unit cell model are used. A pressure load was applied individually to the faces perpendicular to the 1-direction and 3-directions. The resulting voltage (EPOT) plots are shown in Fig. 19. The same post-processing method used for the unit cell models is applied and the calculated piezoelectric coefficients are summarized in Table 6.

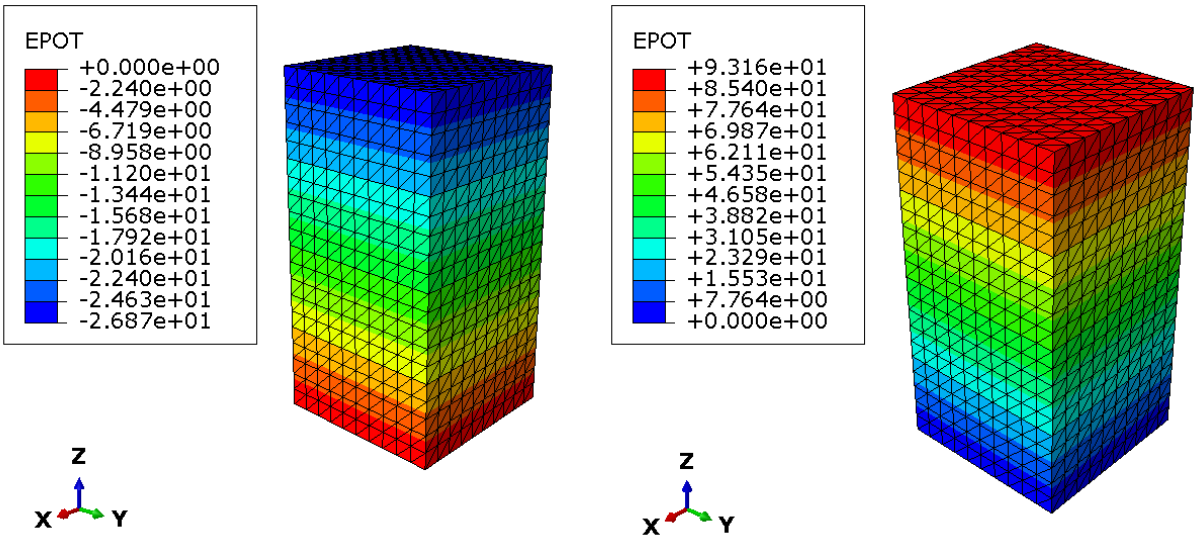

Figure 19. Voltage (EPOT, V) plots for loading in the one-direction (left) and three-direction respectively (right). Loading in the one-direction corresponds to d31 and loading in the 3-direction corresponds to d33.

Table 6. Comparison of Material Property, Analytical, and Numerically Calculated Piezoelectric Coefficients for Bulk Sample

Piezoelectric Coefficient	***Material Property***	***Analytical Model***	***Numerical Model***
d_{31}^{*}	0.27	0.27	0.27
d_{33}^{*}	0.93	0.93	0.93

Based off the results, the simulation results are in strong agreement with the defined material properties and analytical estimates, indicating that the model itself and the post-processing method for obtaining the piezoelectric coefficients is valid.

5.3. Lattice Model for Verification of Periodic Boundary Conditions

Lattice models were created in order to evaluate the assumption that the periodic boundary conditions used in the unit cell are sufficient enough to approximate conditions in an infinite lattice. Due to numerical constraints, a truly infinite lattice model is not possible so a reasonably large finite lattice model is used instead. Long Shu *et al*. found a 5x5x5 unit cell lattice model to be

sufficiently large enough[30]. A 5x5x5 lattice size is used in the present work as well. A lattice composed of 125 unit cells with a plane angle of 120° was arbitrarily selected for this study.

The same PZT composite was used as the base material as in the unit cell models. Tetrahedral C3D10E elements were used to mesh the model. The model was electrically grounded by constraining the electric potential at the bottom flat faces of the lattice to be zero. Rather than directly applying a pressure load, two rigid plates attached to faces on the 1- and 3-direction were used. Usage of the plates ensures parallel displacement in the lattice and also reduces the model set up time. Piezoelectric coefficients were calculated using the averaged voltage values probed from the central unit cell in the lattice. The resulting voltage plots of the lattice model are shown in Fig. 22. The normalized piezoelectric coefficients for the lattice model and corresponding RVE are compared in Table 7.

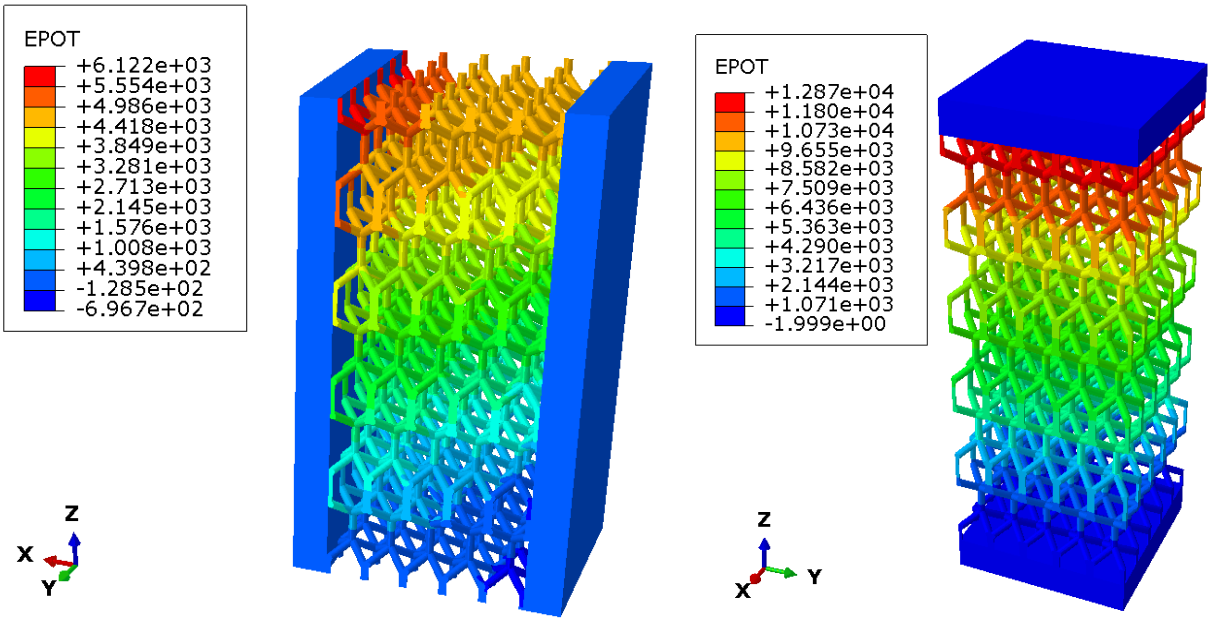

Figure 20. Voltage plot of the 5x5x5 unit cell model[51].

Table 7. Piezoelectric Coefficients of a Θsp = 120° RVE and Lattice Model[51]

Piezoelectric Coefficient	*Unit Cell*	*Lattice*	*Percent Difference*
d_{31}^*	0.46	0.47	2.17%
d_{33}^*	0.77	0.75	2.60%

Based off the results summarized in Table 7, there is strong agreement between the normalized piezoelectric coefficients of the unit cell and lattice model. The small discrepancy between the two models is likely due to the finite size of the lattice model. If the number of unit cells in the lattice model were increased, the discrepancy should decrease. This is behavior is not investigated in the present work due to numerical constraints. Overall, the validity of the unit cell models for predicting the behavior of an infinite lattice is demonstrated.

5.4. Unit Cell Model Results and Discussion

Following the verification of the post-processing technique and boundary conditions of the unit cell models, the piezoelectric coefficients calculated for each unit cell model are presented in Table 8. Fig. 20 contains plots of d_{31}^* and d_{33}^* versus plane angle respectively. Similar trends in plane angle and piezoelectric coefficients can be observed in the plots of numerical results as the analytical results. There is strong agreement between the analytical and numerically calculated normalized piezoelectric coefficients, which reflects positively on the reliability of the two models.

Table 8. Comparison of Analytical and Numerical Piezoelectric Coefficients[51]

Strut Angle (Θ_s)	*Normalized Analytical Coefficient*	*Normalized Numerical Coefficient*
15°	$d_{31}^* = -0.69$	$d_{31} = -0.70$
	$d_{33}^* = 0.19$	$d_{33} = 0.16$
30°	$d_{31}^* = -0.68$	$d_{31} = -0.67$
	$d_{33}^* = 0.27$	$d_{33} = 0.30$

60°	$d_{31}^{*} = -0.46$ $d_{33}^{*} = 0.76$	$d_{31} = -0.44$ $d_{33} = 0.79$
90°	$d_{31}^{*} = -0.28$ $d_{33}^{*} = 0.92$	$d_{31} = -0.25$ $d_{33} = 0.94$
120°	$d_{31}^{*} = 0.48$ $d_{33}^{*} = 0.73$	$d_{31} = 0.46$ $d_{33} = 0.77$
150°	$d_{31}^{*} = 0.64$ $d_{33}^{*} = 0.43$	$d_{31} = 0.63$ $d_{33} = 0.45$
165°	$d_{31}^{*} = 0.69$ $d_{33}^{*} = 0.24$	$d_{31} = 0.68$ $d_{33} = 0.27$

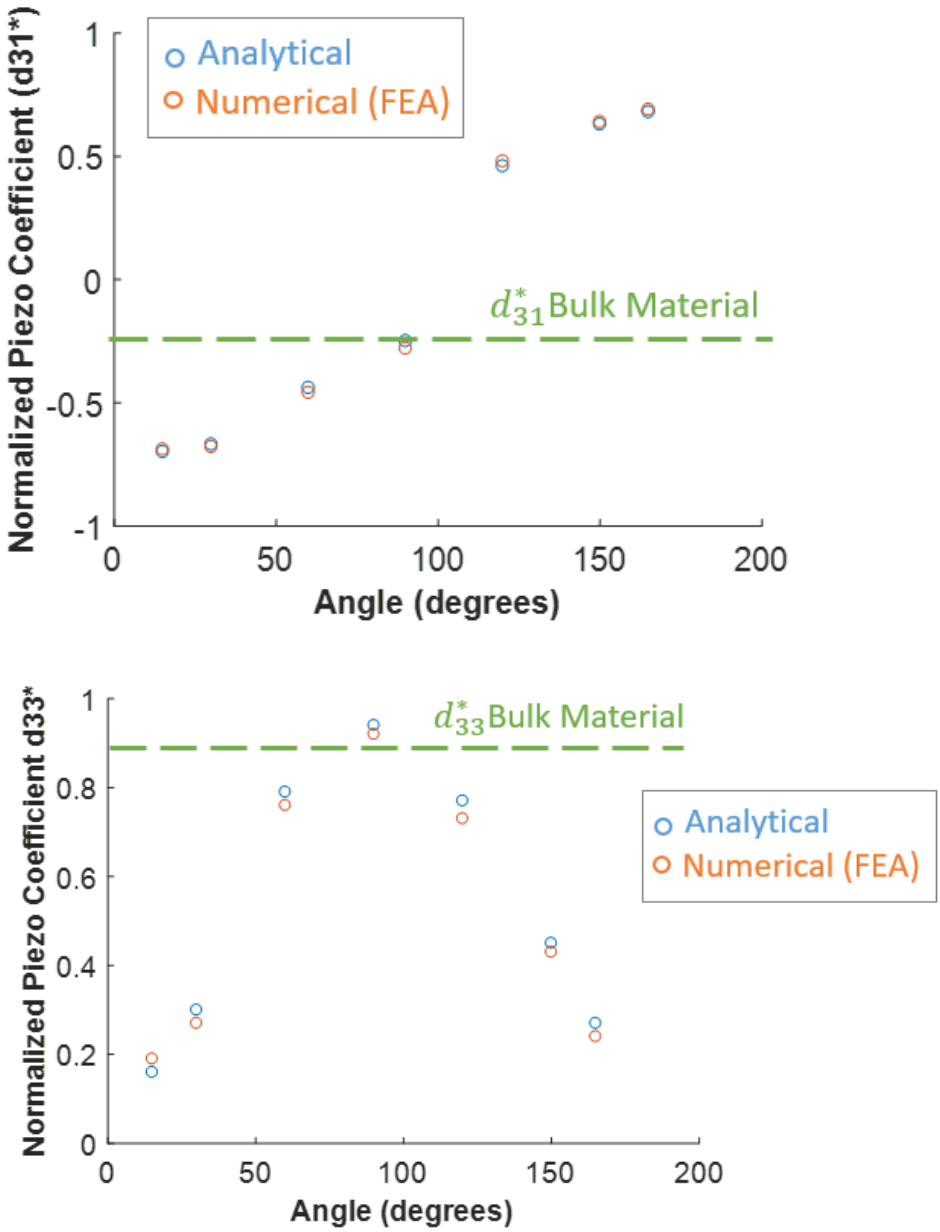

Figure 21. Plot of analytically and numerically calculated d31* (top) and d33* (bottom).

A plot of the unitless d_{31}^* and d_{33}^* vector space using the finite element results is shown in Fig. 21. Again, due to the strong agreement between analytical and numerical models, the same trends are observed in the vector plot as in the analytical vector plot.

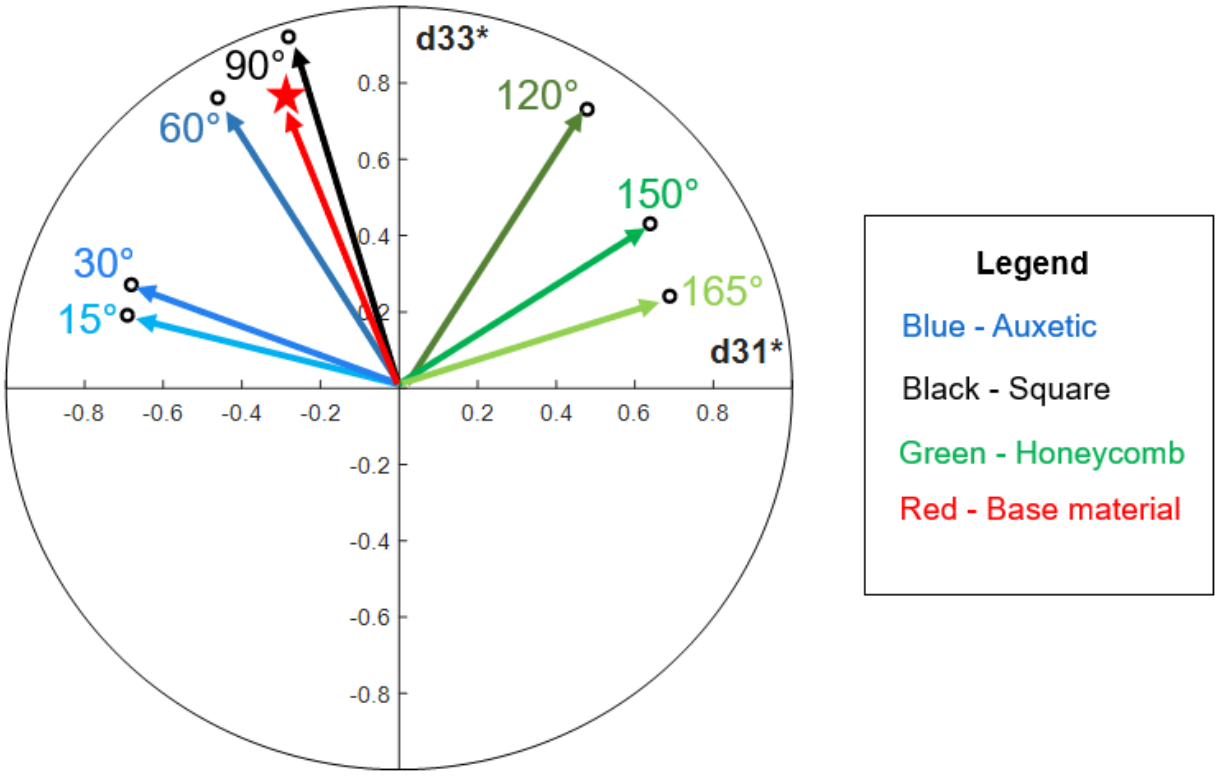

Figure 22. Vector space plot of the numerically calculated d31* and d33*.

5.5. Mesh Convergence

A mesh convergence study was performed on a 3x3x3 lattice model composed of 120° unit cells. A lattice model was used as setting up the periodic boundary conditions for a unit cell model for a very fine mesh would be extremely cumbersome. A 3x3x3 lattice size was deemed large enough for convergence study purposes while having a lower computational cost compared to a 5x5x5 model. Loading and boundary conditions similar to the lattice model used in the previous section are used here. The pressure load applied in the 3-direction was selected.

The results of the mesh convergence study are shown in Fig. 23. The finest mesh is the mesh size used for the lattice models in this work. The low percent difference of 0.008% between the second and third model indicates that the mesh has sufficiently converged and that error arising due to mesh coarseness is sufficiently controlled.

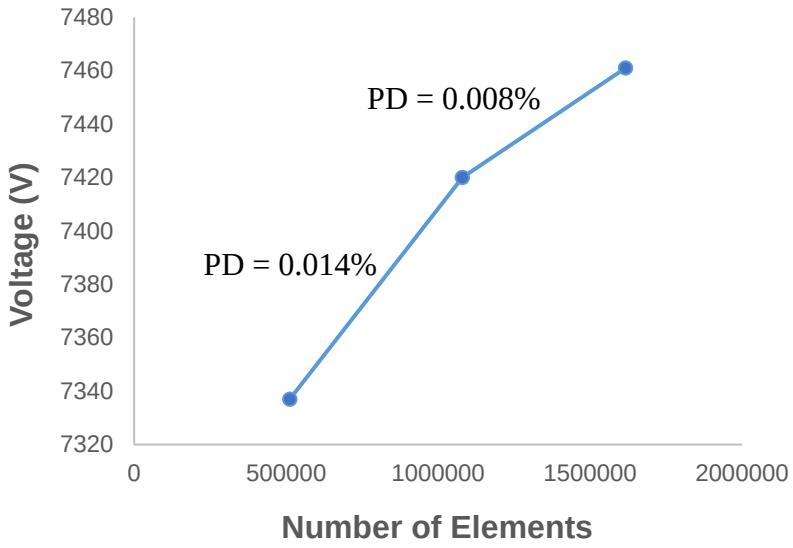

Fig. 23. Mesh convergence of voltage values across three models with an increasingly finer mesh. The percent difference (PD) between sequential models is labelled.

5.6. Numerical Model Discussion

A numerical scheme for modeling and post-processing the piezoelectric composites of ferroelectric unit cell designs was presented. The numerical model was verified through a bulk material block model, a lattice model, and mesh convergence study. Overall, the results of the numerical models are in strong agreement with the analytical model as shown in Fig. 24. This increases the level of confidence in the validity of the analytical predictions and consequently the overall ferroelectric lattice material design and analysis framework. It can be observed that changing the plane angle of the lattice changes the distribution of the piezoelectric coefficients.

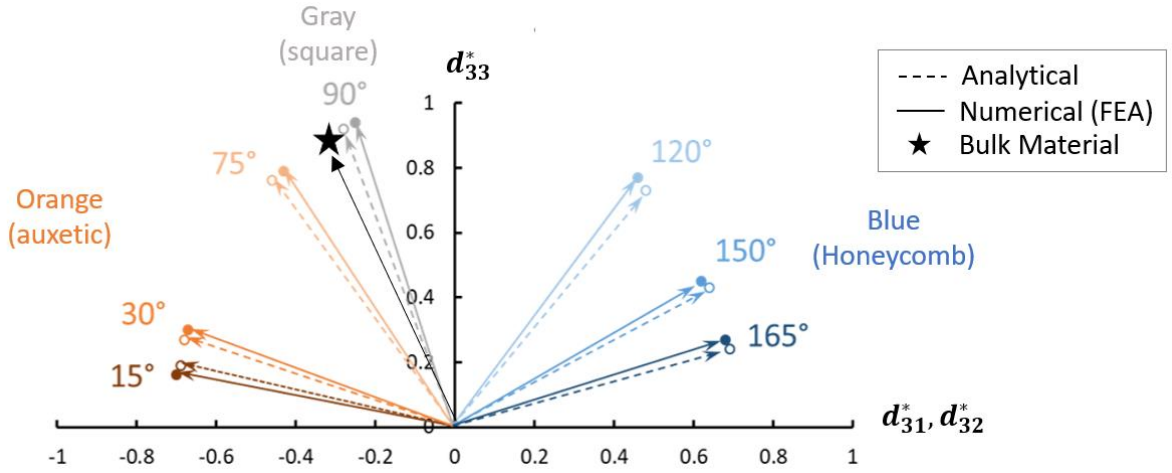

Figure 24. Vector plot of normalized piezoelectric coefficients calculated analytically and using computer simulation[51].

Chapter 6: Experimental Verification and Discussion

Following the analytical and computational analysis, additive manufacturing and experimental testing of the ferroelectric lattice materials is performed using a high-resolution projection micro-stereolithography system and a shaker device integrated with a charge amplifier, respectively. Fig. 25 shows an overview of this process.

Figure 25. Overview of experimental process.

6.1. Additive Manufacturing of Ferroelectric Lattice Materials

Additive manufacturing of the ferroelectric lattice materials is achieved through projection microstereolithography. The working principle behind stereolithography process is selective curing of a photosensitive resin[55]. Ferroelectric properties are introduced to the printed part through addition of ferroelectric material inclusions into the resin. Therefore, the resin itself is a ferroelectric composite material of 0-3 connectivity. Lead zirconante titanate (PZT) nanoparticles are mixed with a printable photopolymer at a range of volume loading (3vol%~50vol%) to obtain a printable ferroelectric composite. PZT nanoparticles were selected due to its high piezoelectric performance, lower cost, and ability to be mixed with a printable resin. Upon completion of print, the lattices are poled in the 3-direction using the Corona poling method[31]. Fig. 26 shows a schematic of the printing process from resin development to final part.

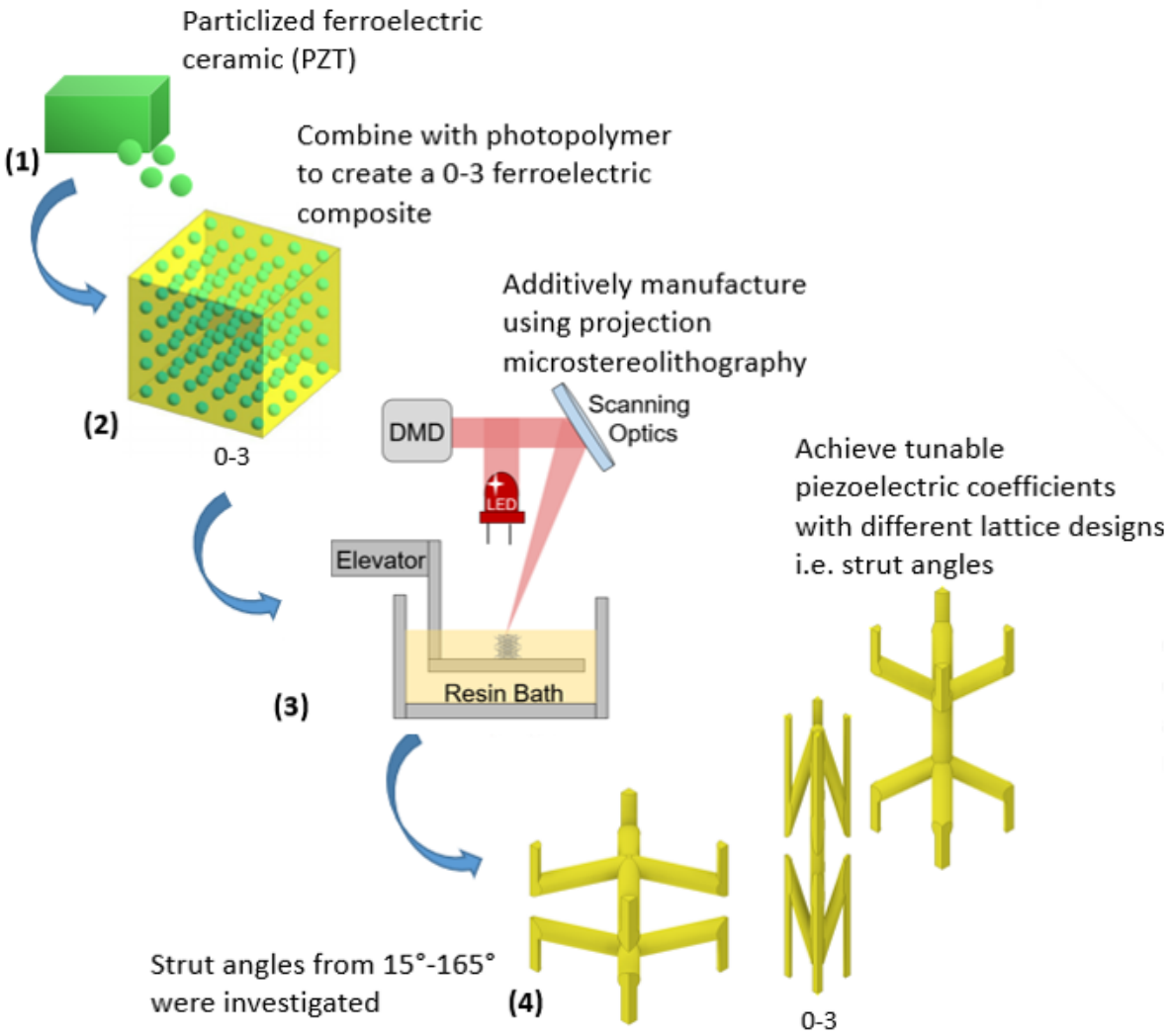

Figure 26. Additive manufacturing process of the ferroelectric lattice materials.

Fig. 27 shows a schematic of the projection microstereolithography system. The CAD model was built in Inventor and sliced to 2D cross-sectional patterns in Netfabb. A digital mirror device (DMD) creates a digital mask of the cross-sectional pattern for each print layer[56]. A LED provides the ultraviolet (UV) light source and is patterned by the DMD. Scanning optics focus the patterned light which selectively cures the photopolymer resin in the resin bath. An elevator moves the print stage vertically as each layer is cured. The high micron-resolution of this printing method allow for small intricate parts such as lattice materials to be printed.

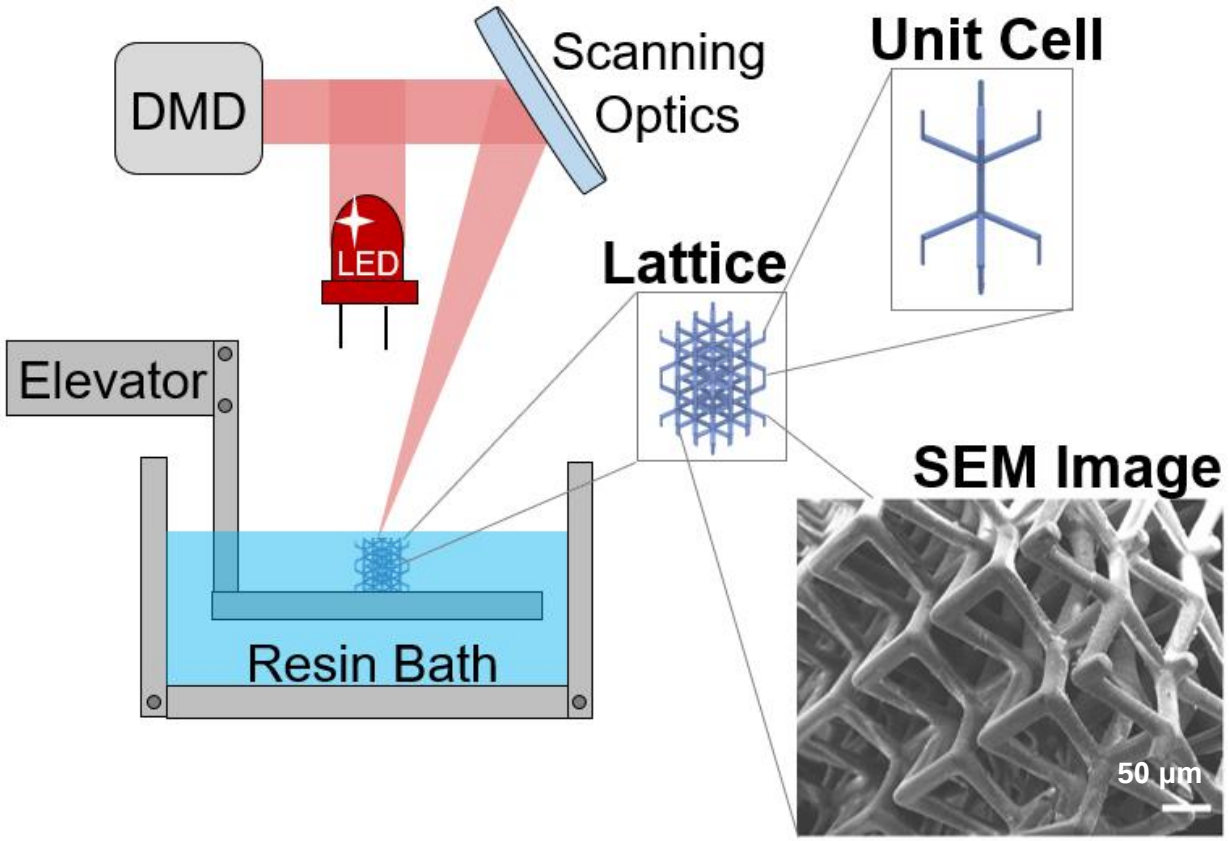

Figure 27. Projection microstereolirhography printing system[51].

6.2. Experimental Testing and Results

Experimental testing of three ferroelectric lattice designs is performed in order to measure their voltage signatures. A force transducer was attached on top of each lattice sample and a shaker was used to cyclically impact (roughly 0.5 N per impact) the lattice. Electrodes and wire leads were attached to the data acquisition system integrated with a resistor (40MΩ) in order to measure the voltage response. Voltage data from experiments on the 75°, 90°, and 120° lattices are shown in Fig. 28.

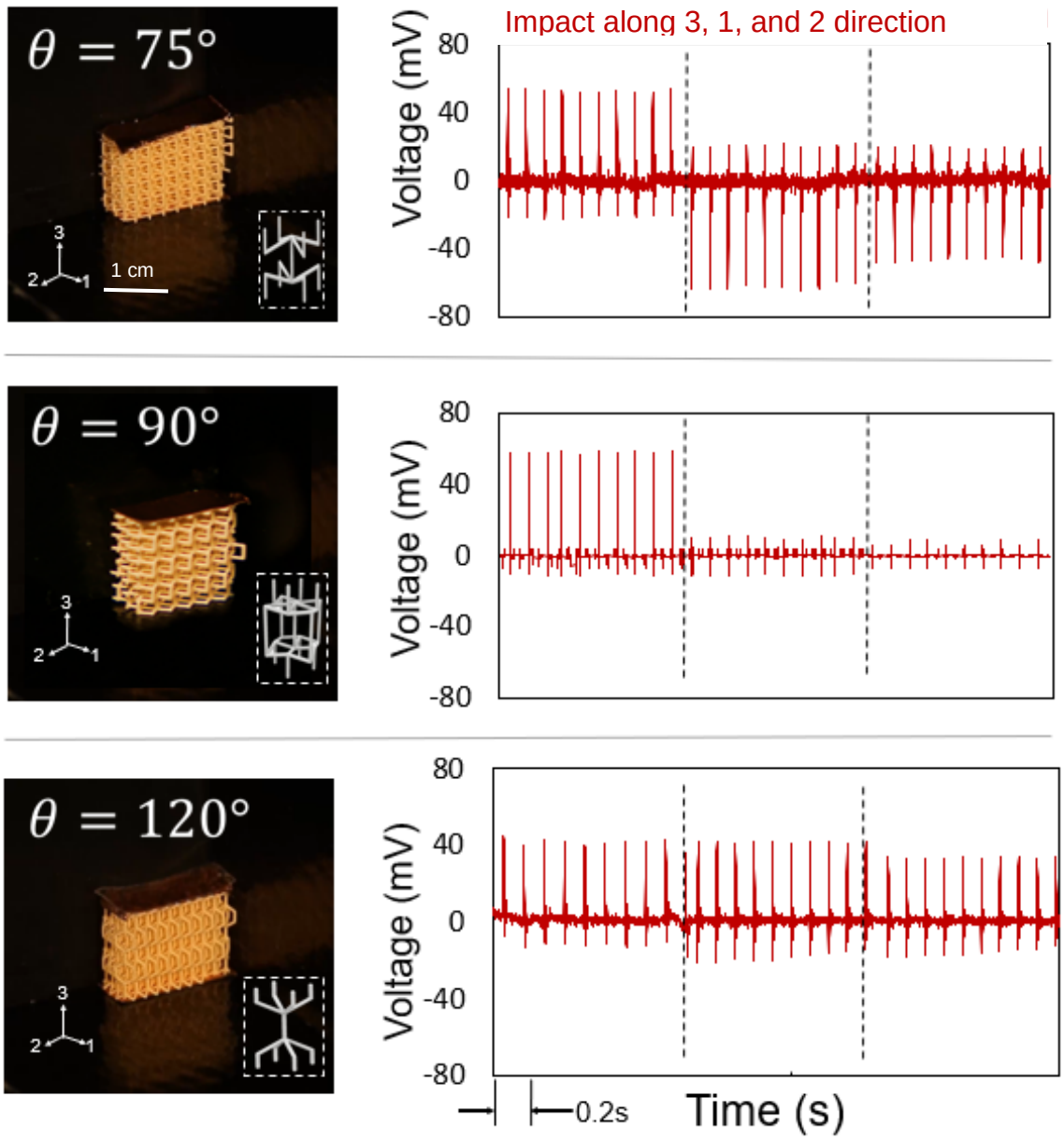

Figure 28. Experimental testing of 75°, 90°, and 120° ferroelectric lattice samples[51].

Despite being printed from the same resin and being subjected to the same loads, the piezoelectric responses of the three lattice materials are different. In this instance, the sign and magnitude of the voltage response correspond directly to the sign and relative magnitude of the piezoelectric coefficients. Therefore, the piezoelectric coefficients of the 75° lattice are {high negative, high negative, and high positive}. the piezoelectric coefficients of the 90° lattice are {high negative, near zero, and near zero}. the piezoelectric coefficients of the 120° lattice are {high positive, high

positive, and high positive}. This leads to the conclusion that this difference in behavior is attributed to solely their different micro-architectures. The key takeaway from these results are summarized in Fig. 29.

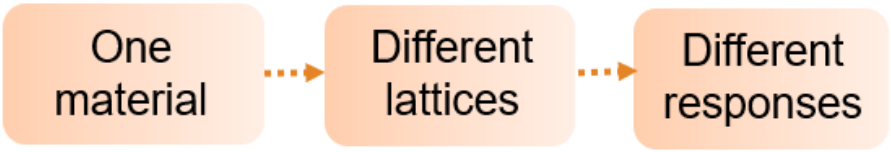

Figure 29. From a single material to new materials with unique responses.

6.3. Discussion of Overall Results

The summarize, at present there are three sets of results: analytical, finite element, and experimental. At the core of these results is the analytical results. A verified analytical method allows for the rational design of architected ferroelectric lattice materials with predictable and tunable piezoelectric coefficients. Therefore, finite element computer models and experimental testing are used to testing and verify values predicted by the analytical model. The models were all found to be in strong agreement in Chapter 5 and Chapter 6, yielding a verified analytical model. The flexibility of the design method and analytical model presented in this work of being capable to be applied to design and model any ferroelectric lattice material fills the existing gap in the literature where there is a lack of a systematic approach to designing new ferroelectric composites. Now that the present method has been verified, practical application of a ferroelectric lattice material as a stress sensor is investigated in the following chapter.

Chapter 7: Application of Ferroelectric Lattice Materials

Real-world application of a ferroelectric lattice materials is demonstrated in the form of a stress sensor. Due to direct piezoelectric effect present in the materials, ferroelectric materials can be used as sensors for pressure, acceleration, and vibration[57] [58]. Ferroelectric sensors offer the advantage of being passive sensors, meaning that they do not require a power source.

There are many types of commercial stress or pressure sensors including piezoresistive strain gauge, capacitive, piezoelectric, or optic to name a few. However, commercial stress sensors capable of multi-directional sensing are often bulky in geometry and size. An array of smaller sensors may be used place of a single larger sensor, but this poses several disadvantages. For instance, multiple sensors would require additional wires or leads. Moreover, it may not be possible to sense stress in multiple directions at a single point as this would require the sensors to be stacked on top of each other and this is not always possible. The geometries of the sensors are also not tailorable, making them unsuitable for certain applications due to size or geometric constraints. These limitations motivate the following work on application of a ferroelectric lattice material as a multi-directional stress sensor.

7.1. Ferroelectric Multi-Directional Stress Sensor Design

A lattice design is proposed here for application as a ferroelectric multi-stress sensor in Fig. 30. Note this design departs from the previously studied auxetic/square/honeycomb lattice because the previous structures were found to be unsuitable for multi-directional sensing applications due to their symmetric geometry.

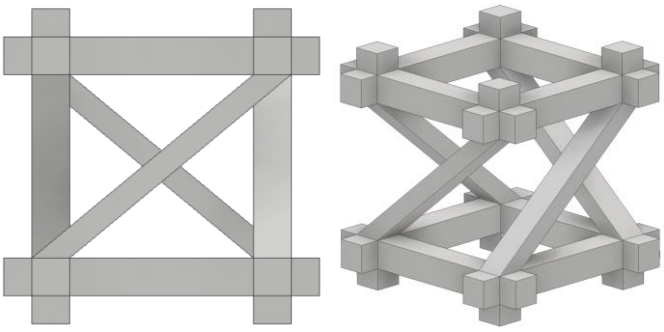

Figure 30. Multi-directional stress sensor unit cell design side and isometric views.

The working principle behind this sensor is that the combination of stresses, and consequently the combination of measured voltages from each angled strut within the unit cell will differ for different stress states, giving a unique voltage signature for each stress state. For instance, for a compressive force applied onto the unit cell in the 3-direction, all four struts are in compression and will have a positive voltage of similar magnitude. For tension in the 3-direction, the struts will have a negative voltage of similar magnitude. For shear in the 5-direction, opposite struts on the 1- and 2- faces will have the same voltage sign and magnitude. i.e. the red and green struts versus the blue and yellow struts in Fig. 31. In a way, the sensor can be viewed as an array of sensors itself, where each of the angled struts is its own sensor. However, the sensor has the advantage of already being pre-assembled and having close-proximity between the sub-sensors. Based off the combination of voltage readings from each strut (V_i) and the difference in voltages between two struts ($\Delta_{i,j}$), it is possible to differentiate between stress modes.

This sensor has advantages over a traditional array in that its components are preassembled and can be made to be much smaller than a traditional sensor. In addition, the unit cell can be tessellated into any geometry that suits the rest of the structure. Table 9 contains predicted voltage outputs in each strut for different stress states. Note, $+/-\sigma_3$ is tension/compression in the 3-direction while $+/-\sigma_5$ is positive/negative shear in the xz-plane. In order to evaluate the predicted voltages, finite element modelling and experimental testing are performed in the following sections.

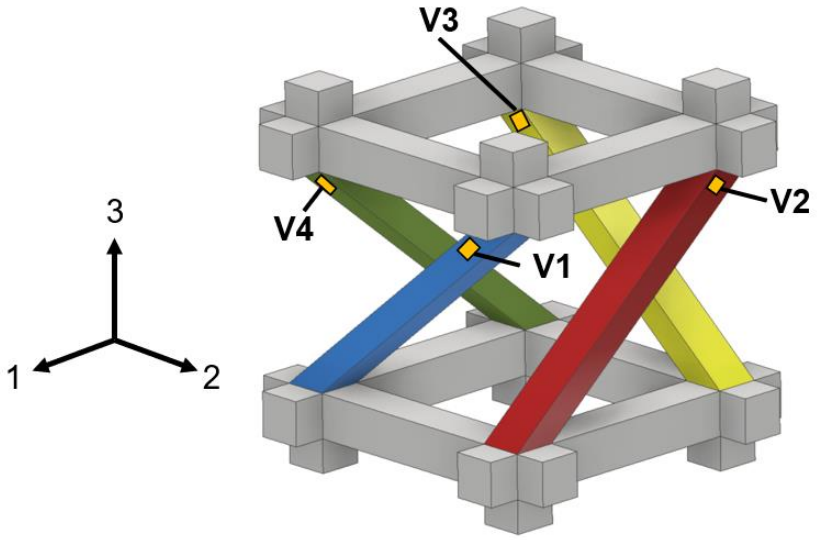

Figure 31. Multi-sensor model. Voltage is measured from each angled strut at the electrode.

Table 9. Predicted Voltage Signatures of Different Stress States

Stress	Symbol	V1	V2	V3	V4
Compression, 3-direction	$-\sigma_3$	+	+	+	+
Tension, 3-direction	σ_3	-	-	-	-
Negative Shear, xz-plane	$-\sigma_5$	+	+	-	-
Positive Shear, xz-plane	σ_5	-	-	+	+

7.2. Ferroelectric Multi-directional Stress Sensor Finite Element Modeling

Finite element analysis in Abaqus 6.14 is performed on the sensor in order to characterize the voltage signature for different stress states. A 2x2x1 unit cell model was used. The model is electrically grounded at the bottom face and is also fixed in the 1-, 2-, and 3- directions on this face. Pressure loads are applied to the top face of the sensor and the same magnitude of pressure is used for each case. The model uses the same material properties as those in Table 4 and Table 5 and is meshed with C3D10E elements. Select cases of the finite element results are included in Fig. 32. Table 10 summarizes the voltage signatures obtained from the finite element models for different stress states.

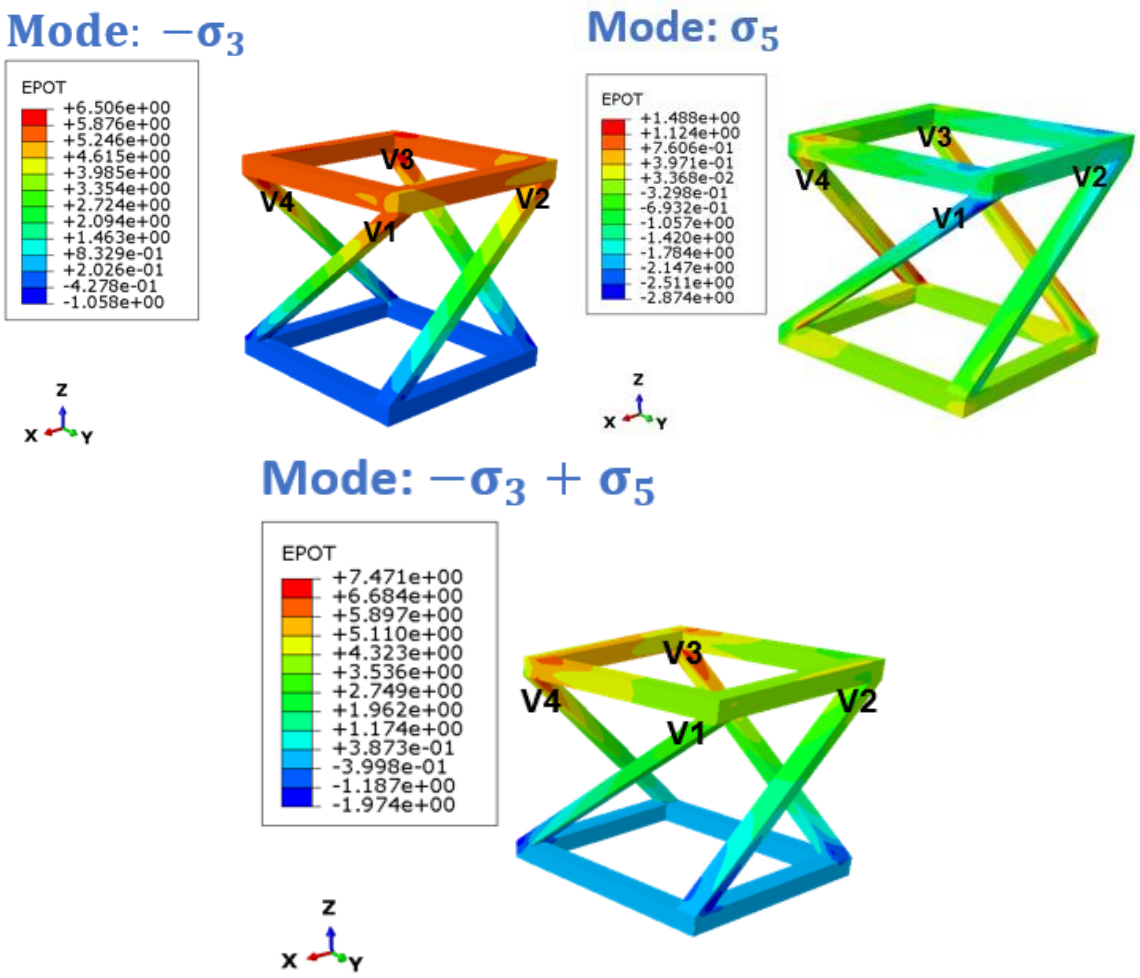

Figure 32. Finite element voltage plots of the ferroelectric sensor for various stress modes.

Table 10. Voltage Signatures of Different Stress States

Stress type	Stress direction	Symbol	V1	V2	V3	V4	$\Delta_{1,2}$
Axial	-z	$-\sigma_3$	+	+	+	+	+
Axial	z	σ_3	-	-	-	-	+
Shear	-xz	$-\sigma_5$	+	+	-	-	+
Shear	xz	σ_5	-	-	+	+	-
Combined	-z & xz	$-\sigma_3 + \sigma_3$	+	+	+	+	+

Based off of the voltage signatures in Table 10, it is possible to differentiate between certain axial, shear, and combined stress states as each stress state has a distinct combination of V1, V2, V3, V4, and $\boldsymbol{\Delta_{1,2}}$ signatures. The $\boldsymbol{\Delta_{1,2}}$ parameter is calculated in Eqn (22) by

$$\boldsymbol{\Delta_{1,2}} = V1 - V2 \tag{22}$$

In addition, the magnitude of the stress can be calculated using a modified version of the analytical framework presented in Chapter 3. In the next section, the sensor is additively manufactured and tested.

7.3. Ferroelectric Multi-sensor Experimental Verification

The sensor design was additively manufactured using projection microstereolithography and poled in the z-direction using the Corona poling method. The sensor was grounded at the bottom face and four electrodes were attached a unit cell within the lattice in order to take voltage measurements. The experimental setup is shown in Fig. 33.

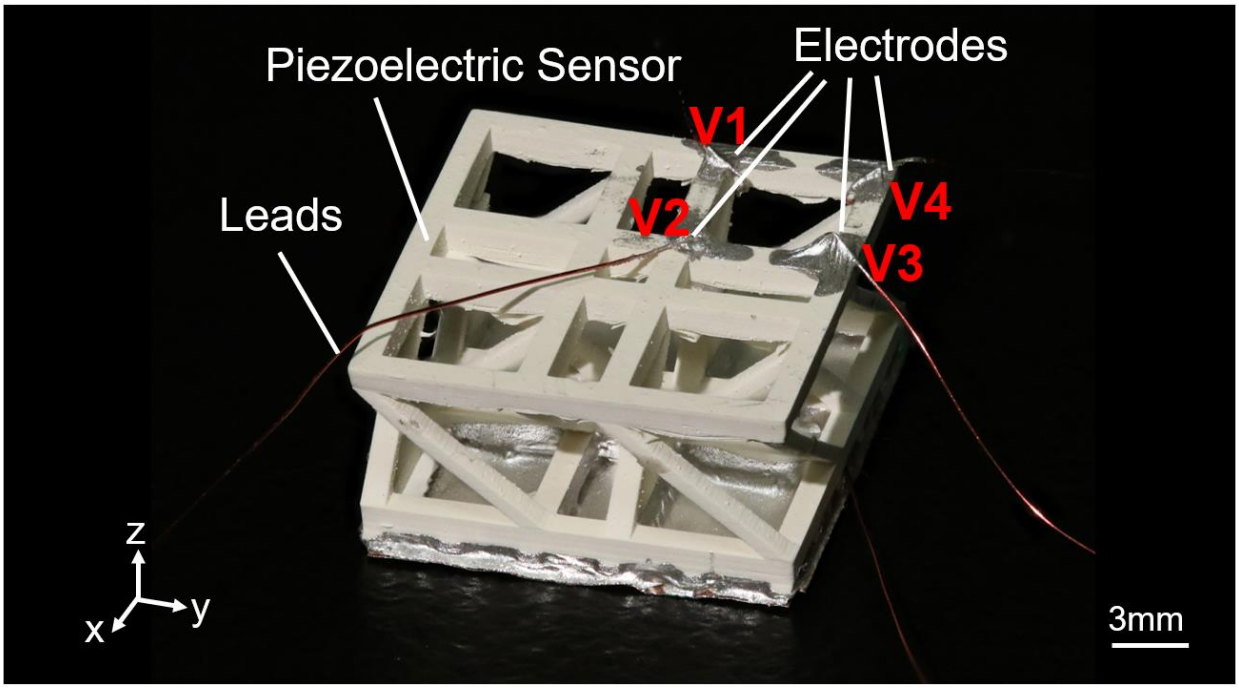

Figure 33. The printed multi-stress sensor. Photograph by H. Cui.

Experimental testing of the sensor is achieved through a shaker and impulse hammer testing fixture. The shaker creates the impact force while the hammer, shown in Fig. 34, measures the impact. The experimentally measured voltages are summarized and compared to those from the finite element model in Table 11. Strong agreement between the voltage signatures was found between finite element and experimental results. Thus, this sensor is a viable multi-stress sensor and offers advantages over commercial multi-stress sensors due to its small size, preassembled housing, and customizable geometry.

Table 11. Comparison of Voltage Signatures from FEA and Experimental Results

	Stress	V1	V2	V3	V4
FEA	$-\sigma_3$	+	+	+	+
	σ_5	-	-	+	+
Experimental	$-\sigma_3$	+	+	+	+
	σ_5	-	-	+	+

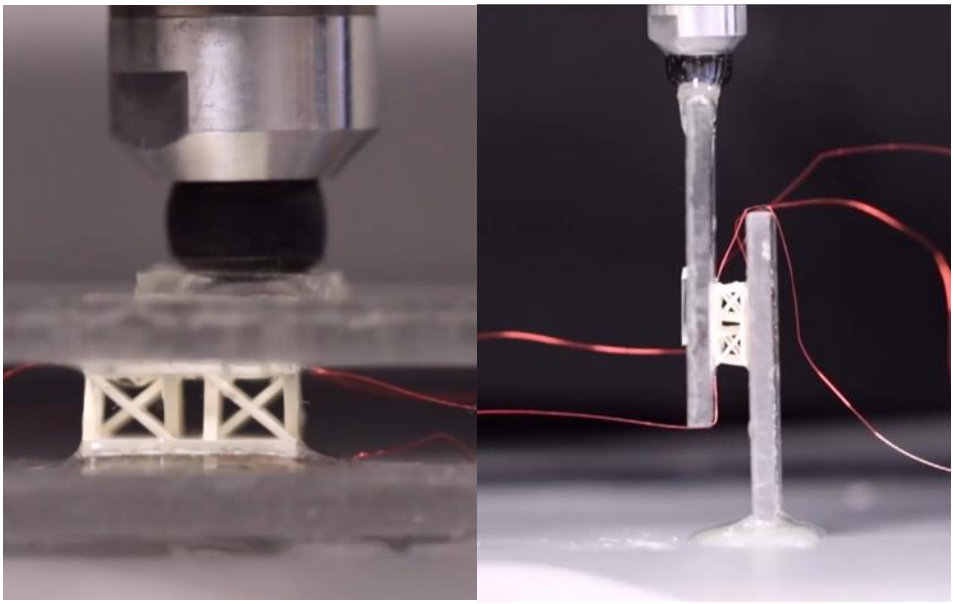

Figure 34. Experimental testing of the multi-sensor for compression (left) and shear (right) stress states. Photograph and experimental testing by H. Cui.

Chapter 8: Conclusion

8.1. Conclusion

In conclusion, the design, analysis, and application of architected ferroelectric lattice materials is presented. The lack of a design and analysis framework for ferroelectric lattice materials was identified in the literature and was developed in response. The unit cell design parameter chosen for this work is the plane angle but any geometric parameter of the unit cell could be selected, allowing for a high amount of design freedom and design possibilities as discussed in Chapter 3. An analytical method based on beam theory and a volume-averaging scheme is used in Chapter 4. This analytical framework was verified with finite element models and experimental testing in Chapter 5 and Chapter 6 respectively. Unit cell and lattice finite element models are used. Experimental testing of the ferroelectric lattice material designs are achieved through first additively manufacturing the lattices and then performing testing with a shaker device. The framework developed in this work allows for the rational design of ferroelectric lattice materials whose piezoelectric properties are tunable through micro-architecture of the lattice structure.

The significance of these results is that it then becomes possible to start with a single ferroelectric material and use that material to additively manufacture an infinite number of new, architected lattice materials whose piezoelectric coefficients are simultaneously unique from the base material and from each other. In addition, application of the ferroelectric lattice material as a multi-sensor is presented. This sensor has advantages over commercially available sensors because of its small size, customizable geometry, and multi-sensing capabilities.

8.2. Future Work

Some topics of interest for future work are exploration of additional lattice designs, simultaneous characterization of the mechanical properties of the ferroelectric lattice materials, and application of the lattice materials for different roles. In the scientific literature, there exists many well-studied lattice designs such as the octet truss, kagome, or chiral structures. But beyond the scientific literature, intricate lattice designs can be found in the art and history of many cultures. It would be interesting to use these designs as inspiration for new, complex lattice designs capable of unique properties.

In addition, characterization and tuning of the piezeoelectric properties of the lattice materials were the focus of the present work so architectural effects on mechanical or other electrical properties were not considered. In reality, changes in architecture will also result in changes in other mechanical and electrical properties. It would be interesting to also study how these other properties change as the architecture is changed and be able to optimize a group of material properties for a specific applciation.

Finally, as mentioned in the introduction, ferroelectric materials have many modern applications. Sensors are one such example, but there are many more applications such as actuators or energy harvesters. Different applications may have different combinations of piezoelectric coefficients that are optimal for that application, making the highly customizable ferroelectric lattice materials studied in this work very useful. Overall, the present work opens up exciting new possibilities for the design of smart materials.

References

[1] D. Damjanovic, P. Muralt, and N. Setter, Ferroelectric Sensors. 2001, pp. 191-206.

[2] U. Kushnir and O. Rabinovitch, Advanced piezoelectric–ferroelectric stack actuator. 2009, pp. 102-109.

[3] S. Herold and D. Mayer, "Adaptive Piezoelectric Absorber for Active Vibration Control," Actuators, vol. 5, no. 1, 2016.

[4] D. C. Fei Sun, "Ferroelectrics for Biomedical Applications," 2017.

[5] H. Huang et al., "Elastic and Electric Damping Effects on Piezoelectric Cantilever Energy Harvesting," Ferroelectrics, vol. 459, no. 1, pp. 1-13, 2014/01/03 2014.

[6] M. Davis, D. Damjanovic, D. Hayem, and N. Setter, "Domain engineering of the transverse piezoelectric coefficient in perovskite ferroelectrics," vol. 98, no. 1, p. 014102, 2005.

[7] S.-H. Shin, Y.-h. Kim, M. H. Lee, J.-Y. Jung, J. Hun Seol, and J. Nah, Lithium-Doped Zinc Oxide Nanowires-Polymer Composite for High Performance Flexible Piezoelectric Nanogenerator. 2014.

[8] K. L. Jim, C. W. Leung, S. T. Lau, S. H. Choy, and H. L. W. Chan, "Thermal tuning of phononic bandstructure in ferroelectric ceramic/epoxy phononic crystal," Applied Physics Letters, vol. 94, no. 19, p. 193501, 2009/05/11 2009.

[9] V. Y. Topolov, Bisegna, P, Bowen, C R, Piezo-active composites orientation effects and anisotropy factors (Springer Series in Materials Science). Berlin, Germany: Springer, 2014.

[10] P. Kanouté, D. P. Boso, J. L. Chaboche, and B. A. Schrefler, "Multiscale Methods for Composites: A Review," Archives of Computational Methods in Engineering, vol. 16, no. 1, pp. 31-75, 2009/03/01 2009.

[11] J.-L. L. Alain Bensoussan, George Papanicolaou, Asymptotic Analysis for Periodic Structures. Elsevier, 1978, p. 700.

[12] M. L. Dunn and M. Taya, "Micromechanics predictions of the effective electroelastic moduli of piezoelectric composites," International Journal of Solids and Structures, vol. 30, no. 2, pp. 161-175, 1993/01/01/ 1993.

[13] A. Almusallam et al., "Flexible piezoelectric nano-composite films for kinetic energy harvesting from textiles," Nano Energy, vol. 33, pp. 146-156, 2017/03/01/ 2017.

[14] T. Fey et al., "Mechanical and electrical strain response of a piezoelectric auxetic PZT lattice structure," Smart Materials and Structures, vol. 25, no. 1, p. 015017, 2015/12/02 2015.

[15] G. Bai, R. Li, Z. G. Liu, Y. D. Xia, and J. Yin, "Tuned dielectric, pyroelectric and piezoelectric properties of ferroelectric P(VDF-TrFE) thin films by using mechanical loads," Journal of Applied Physics, vol. 111, no. 4, p. 044102, 2012/02/15 2012.

[16] S.-i. Park, D. Rosen, S.-K. Choi, and C. Duty, Effective Mechanical Properties of Lattice Material Fabricated by Material Extrusion Additive Manufacturing. 2014.

[17] X. Zheng et al., "Ultralight, ultrastiff mechanical metamaterials," Science, vol. 344, no. 6190, p. 1373, 2014.

[18] H. S. Kim and S. T. S. Al-Hassani, "Effective elastic constants of two-dimensional cellular materials with deep and thick cell walls," International Journal of Mechanical Sciences, vol. 45, no. 12, pp. 1999-2016, 2003/12/01/ 2003.

[19] C. Chu, G. Graf, and D. W. Rosen, "Design for Additive Manufacturing of Cellular Structures," Computer-Aided Design and Applications, vol. 5, no. 5, pp. 686-696, 2008/01/01 2008.
[20] M. Doyoyo and J. W. Hu, "Multi-axial failure of metallic strut-lattice materials composed of short and slender struts," International Journal of Solids and Structures, vol. 43, no. 20, pp. 6115-6139, 2006/10/01/ 2006.
[21] H. Tollenaere and D. Caillerie, "Continuous modeling of lattice structures by homogenization," Advances in Engineering Software, vol. 29, no. 7, pp. 699-705, 1998/08/01/ 1998.
[22] L. Guo, T. Bashir, E. Bresky, and N. K. Persson, "28 - Electroconductive textiles and textile-based electromechanical sensors—integration in as an approach for smart textiles," in Smart Textiles and their Applications, V. Koncar, Ed. Oxford: Woodhead Publishing, 2016, pp. 657-693.
[23] A. Arnau and D. Soares, "Fundamentals of Piezoelectricity," in Piezoelectric Transducers and Applications, A. A. Vives, Ed. Berlin, Heidelberg: Springer Berlin Heidelberg, 2008, pp. 1-38.
[24] M. de Jong, W. Chen, H. Geerlings, M. Asta, and K. A. Persson, "A database to enable discovery and design of piezoelectric materials," Scientific Data, Data Descriptor vol. 2, p. 150053, 09/29/online 2015.
[25] V. Y. Topolov, E. I. Bondarenko, A. V. Turik, and A. I. Chernobabov, "The effect of domain structure on electromechanical properties of PbTiO3,-based ferroelectrics," Ferroelectrics, vol. 140, no. 1, pp. 175-181, 1993/02/01 1993.
[26] V. Y. Topolov, A. V. Turik, and A. I. Chernobabov, On the mechanism of high piezoelectric anisotropy in lead titanate-based ferroelectrics. 1994.
[27] D. Maurya, N. Wongdamnern, R. Yimnirun, and S. Priya, "Dielectric and ferroelectric response of compositionally graded bilayer and trilayer composites of BaTiO3 and 0.975BaTiO3–0.025Ba(Cu1/3Nb2/3)O3," Journal of Applied Physics, vol. 108, no. 12, p. 124111, 2010/12/15 2010.
[28] J. Kim, K. J. Loh, and J. P. Lynch, Piezoelectric polymeric thin films tuned by carbon nanotube fillers (SPIE Smart Structures and Materials + Nondestructive Evaluation and Health Monitoring). SPIE, 2008.
[29] N. Mallik and M. C. Ray, "Effective Coefficients of Piezoelectric Fiber-Reinforced Composites," vol. 41, no. 4, pp. 704-710, 2003.
[30] L. Shu, R. Liang, Y. Yu, T. Tian, Z. Rao, and Y. Wang, "Unique elastic, dielectric and piezoelectric properties of micro-architected metamaterials," Journal of Materials Chemistry C, 10.1039/C8TC05847D vol. 7, no. 9, pp. 2758-2765, 2019.
[31] H. Kim, F. Torres, Y. Wu, D. Villagran, Y. Lin, and T.-L. Tseng, "Integrated 3D printing and corona poling process of PVDF piezoelectric films for pressure sensor application," Smart Materials and Structures, vol. 26, no. 8, p. 085027, 2017/07/13 2017.
[32] V. Yuryevich Topolov and C. Bowen, Electromechanical Properties in Composite Based on Ferroelectrics. 2009.
[33] B. Jiang, D.-N. Fang, and K.-C. Hwang, "A unified model for piezocomposites with non-piezoelectric matrix and piezoelectric ellipsoidal inclusions," International Journal of Solids and Structures, vol. 36, no. 18, pp. 2707-2733, 1999/06/01/ 1999.
[34] M. L. Dunn and M. Taya, "Electromechanical Properties of Porous Piezoelectric Ceramics," vol. 76, no. 7, pp. 1697-1706, 1993.

[35] M. L. Dunn, "Micromechanics of coupled electroelastic composites: Effective thermal expansion and pyroelectric coefficients," Journal of Applied Physics, vol. 73, no. 10, pp. 5131-5140, 1993/05/15 1993.
[36] L. Khoroshun, B. Maslov, and P. V. Leshchenko, Prediction of the effective properties of piezoactive composite materials. 1989.
[37] V. M. Levin, M. I. Rakovskaja, and W. S. Kreher, "The effective thermoelectroelastic properties of microinhomogeneous materials," International Journal of Solids and Structures, vol. 36, no. 18, pp. 2683-2705, 1999/06/01/ 1999.
[38] N. Fakri, L. Azrar, and L. El Bakkali, Electroelastic behavior modeling of piezoelectric composite materials containing spatially oriented reinforcements. 2003, pp. 361-384.
[39] D. S. Nguyen and F. Vignat, "A method to generate lattice structure for Additive Manufacturing," in 2016 IEEE International Conference on Industrial Engineering and Engineering Management (IEEM), 2016, pp. 966-970.
[40] D. W. Rosen, "Computer-Aided Design for Additive Manufacturing of Cellular Structures," Computer-Aided Design and Applications, vol. 4, no. 5, pp. 585-594, 2007/01/01 2007.
[41] L. Yang, O. Harrysson, H. West, and D. Cormier, "Mechanical properties of 3D re-entrant honeycomb auxetic structures realized via additive manufacturing," International Journal of Solids and Structures, vol. 69-70, pp. 475-490, 2015/09/01/ 2015.
[42] S. M. Ahmadi et al., "Mechanical behavior of regular open-cell porous biomaterials made of diamond lattice unit cells," Journal of the Mechanical Behavior of Biomedical Materials, vol. 34, pp. 106-115, 2014/06/01/ 2014.
[43] S. Iyer, M. Alkhader, and T. A. Venkatesh, "Electromechanical Response of Piezoelectric Honeycomb Foam Structures," vol. 97, no. 3, pp. 826-834, 2014.
[44] P. W. Bosse, K. S. Challagulla, and T. A. Venkatesh, "Effects of foam shape and porosity aspect ratio on the electromechanical properties of 3-3 piezoelectric foams," Acta Materialia, vol. 60, no. 19, pp. 6464-6475, 2012/11/01/ 2012.
[45] T. Shimada, L. V. Lich, K. Nagano, J. Wang, and T. Kitamura, "Hierarchical ferroelectric and ferrotoroidic polarizations coexistent in nano-metamaterials," Scientific Reports, Article vol. 5, p. 14653, 10/01/online 2015.
[46] J. Shi and A. H. Akbarzadeh, Architected Cellular Piezoelectric Metamaterials: Thermo-Electro-Mechanical Properties. 2018.
[47] "Shadow Puppet Vectors," ed, 2019, p. Shadow puppets made with the hands.
[48] R. Lakes, "Foam structures with a negative Poisson's ratio," (in English), Science, Article vol. 235, p. 1038+, 1987/02/27/ 1987.
[49] W. Yang, Z.-M. Li, W. Shi, B.-H. Xie, and M.-B. Yang, "Review on auxetic materials," Journal of Materials Science, vol. 39, no. 10, pp. 3269-3279, 2004/05/01 2004.
[50] P. R. Villeneuve and M. Piche´, "Photonic band gaps in two-dimensional square and hexagonal lattices," Physical Review B, vol. 46, no. 8, pp. 4969-4972, 08/15/ 1992.
[51] H. Cui et al., "Three-dimensional printing of piezoelectric materials with designed anisotropy and directional response," Nature Materials, vol. 18, no. 3, pp. 234-241, 2019/03/01 2019.
[52] V. S. Deshpande, N. Fleck, and M. Ashby, Effective Properties of the Octet-Truss Lattice Material. 2001, pp. 1747-1769.

[53] L. Dong, V. Deshpande, and H. Wadley, "Mechanical response of Ti–6Al–4V octet-truss lattice structures," International Journal of Solids and Structures, vol. 60-61, pp. 107-124, 2015/05/15/ 2015.
[54] J. O. Weidong Wu, "Applying Periodic Boundary Conditions in Finite Element Analysis," 2014 SIMULIA Community Conference 2014.
[55] D. W. R. Ian Gibson, Brent Stucker, Additive Manufacturing Technologies Rapid Prototyping to Direct Digital Manufacturing. Springer, 2010.
[56] X. Zheng et al., "Design and optimization of a light-emitting diode projection micro-stereolithography three-dimensional manufacturing system," Review of Scientific Instruments, vol. 83, no. 12, p. 125001, 2012/12/01 2012.
[57] J. M. Herbert, Ferroelectric transducers and sensors (Electrocomponent science monographs,0275-7230 ;v. 3, no. xxv, 437 p.). New York: Gordon and Breach Science Publishers, 1982, pp. xxv, 437 p.
[58] J. W. Waanders, Piezoelectric Ceramics: Properties and Applications. Philips Components, 1991.